4F SERIES PAW PSEUDOPOTENTIALS

by

GÜVEN AKÇAY

THESIS SUBMITTED TO
THE GRADUATE SCHOOL OF NATURAL AND APPLIED SCIENCES
OF
THE ABANT İZZET BAYSAL UNIVERSITY
IN PARTIAL FULFILLMENT OF THE REQUIREMENTS FOR THE
DEGREE OF
MASTER OF SCIENCE
IN
THE DEPARTMENT OF PHYSICS

December 2013

Approval of the Graduate School of Natural Sciences

Prof. Dr. Yaşar Dürüst

Director

I certify that this thesis satisfies all the requirements as a thesis for the degree of Master of Science.

Prof. Dr. Ibrahim Belenli

Head of Physics Department

This is to certify that we have read this thesis and that in our opinion it is fully adequate, in scope and quality as a thesis for the degree of Master of Science.

Assoc. Prof. Dr. Cihan Parlak

Supervisor

Prof. Dr. Resul Eryiğit

Co-advisor

Examining Committee Members

1. Assoc. Prof. Dr. Cihan Parlak .....
2. Prof. Dr. Resul Eryiğit .....
3. Assoc. Prof. Dr. Mustafa Akdoğan .....
4. Assist. Prof. Dr. Tanju Gürel .....
5. Assist. Prof. Dr. Bahadır Altıntaş .....

ABSTRACT

4F SERIES PAW PSEUDOPOTENTIALS

Güven Akçay

Master of Science, Department of Physics

Supervisor: Assoc. Prof. Dr. Cihan Parlak

Co-advisor: Prof. Dr. Resul Eryiğit

December 2013, 91 pages

4f electrons show peculiar behaviour leading to many interesting optical, magnetic, electrical and structural solid state phenomena. Their description in a pseudopotential framework proved to be difficult, partly due to their compact structure. The aim of the present thesis is to provide a well-tested of Projected Augemented Wave (PAW) data set for 4f electron system that can be used in solid state codes to investigate the properties of rare-earth containing solids. The projected augemented wave data sets for the lanthanide group of elements were created with local-density as well as gradient-corrected exchange correlations. The set of these PAWs were used to calculate equilibrium structural data such as lattice constant, bulk modulus, and its' pressure derivative of 15 lanthanide elements (La, Ce, Pr, Nd, Pm, Sm, Eu, Gd, Tb, Dy, Ho, Er, Tm, Yb and Lu). We have also calculated electronic band structure and angular momentum resolved density of electronic states. The computed results show a reasonable agreement with the available data. The outcome of the thesis is 15 sets of LDA and GGA PAW data for lanthanides that can be used to describe rare-earths in any compound that contains them.

Keywords: Density Functional Theory (DFT), Projector Augemented Wave, Pseudopotential, Lanthanides and 4f Electron Sysytems.

ÖZET

4F SERİSİ YZD SANALPOTANSİYELLERİ

Güven Akçay

Yüksek Lisans, Fizik Bölümü

Tez Danışmanı: Doç. Dr. Cihan Parlak

Yardımcı Tez Danışmanı: Prof. Dr. Resul Eryiğit

Aralık 2013, 91 sayfa

4f elektronları birçok ilginç optik, manyetik, elektriksel ve yapısal katı hal olaylarına sebep olan olağandışı davranış gösterir. Bu elektronların sanalpotansiyel çerçevede açıklanması karmaşık yapıları nedeni ile kısmen zordur. Bu tezin amacı, nadir toprak elementi içeren katıların özelliklerini araştırmak amacı ile katı hal kodlarında kullanılan 4f elektron sistemleri için çok iyi test edilmiş bir Yansıtıcı ile Zenginleştirilmiş Dalga (YZD) veri kümesi oluşturmaktır. Lantanit grubu elementler için YZD veri kümeleri hem Yerel Yoğunluk Yaklaşımı hem de Genel Gradyan Yaklaşımı değiş-tokuş korelasyonlar için oluşturuldu. Lantanit grubu elementleri için YZD veri kümeleri örgü sabiti, hacim modülü ve hacim modülünün basınca göre türevini hesaplamak için kullanıldı. Ayrıca elektronik durum yoğunluğu, açısal momentum bağımlı elektronik durum yoğunluğu ve elektronik bant yapısı da hesaplandı. Elde edilen sonuçlar var olan verilerle uygunluk göstermektedir. Bu tezin sonunda 15 lantanit elementinin Yerel Yoğunluk Yaklaşımı ve Genel Gradyan Yaklaşımının YZD verileri, nadir toprak elementi içeren herhangi bir bileşiği tanımlamak için kullanılabilir.

Anahtar Kelimeler: Yoğunluk Fonksiyonel Teorisi (YFT), Yansıtıcı ile Zenginleştirilmiş Dalga (YZD), Sanalpotansiyel, Lantanitler ve 4f Elektronlu Sistemler.

ACKNOWLEDGEMENTS

I express sincere appreciation to my advisors, Prof. Dr. Resul Eryiğit and Assoc. Prof. Dr. Cihan Parlak for their guidance, encouragement and support of this study. I also thank their for their inexhaustible patience, tolerance and trust at me.

I also express sincere appreciation to Assist. Prof. Dr. Tanju Gürel, Assist. Prof. Dr. İsmail Uğur Tiryaki and Assist. Prof. Dr. Önder Şimşek for his suggestions and contributions. Also, my thanks expert Elvan Kuzeytepe and assistant Tolga Asaf Ülgen due to his help and support during this work.

I would like to thank My Friends, Eren Haydan, Abdulkadir Gezer, Uğur Zağ, colleagues and all my teachers in mathematics department and in physics department for their friendship and encouragement all trough my years at AIBU.

Especially, thanks to My Parents, My Father Ziyeddin Akçay, My Mother Gülten Akçay, My Nephews Ömer and Sema, My Teachers Dursun Karaboğa and Koray Köçgen, and Assist. Prof. Dr. Hale Gonce Köçgen for their love, trust and help. They encouraged me in all phases of my life.

This work was supported by the Scientific and Technological Research Council of Turkey (TUBITAK) under grant no TBAG-111T796. The support is gratefully acknowledged

To My Family ...

TABLE OF CONTENTS

LIST OF TABLES

LIST OF FIGURES

CHAPTER 1

INTRODUCTION

In the last century, electronic structure calculations have made very important contributions to our insigth into solid-state properties of materials. These calculations depend on the local density approximation (LDA) of the density-functional theory (DFT). The density functional theory, which experience an effective potential maps the ground state of an interacting electron gas onto the ground state of noninteracting electrons. In addition to this, the first used method Kohn-Sham density functional method [1, 2], which uses a plane wave basis set and the pseudopotential (PSP) approximation is the most successful method for computational material science recently. The major contribution of this method is fair simple, but determination of their behavior by standard norm-conserving pseudopotentials of some elements, e.g. first row elements, transition metals, and rare earth elements, are not very cheap [3, 4]. So, many technique have been experimented to generate soft pseudopotentials. It is known that many techniques were used to generate soft pseudopotentials electronic structure methods for electronic structure calculation.

The widely used electronic structure methods can be turned into two types: (1) the linear methods improved by Andersen from the augmented-plane-wave (APW) method and the Korringa-Kohn-Rostocker method and (2) the pseudopotential method relying on norm-conserving ab initio pseudopotentials invented by Hamann, Schluter and Chiang (HSC) [5, 6]. One another hands, the Gaussian basis sets to expand the full wave functions is used in chemistry [6]. The linear methods can be subdivided into a variety of methods ranging from the most accurate linear augmented-plane-wave (LAPW) method to the linear muffin-tin orbital (LMTO) method, which are fairly a simplified version for electronic struc-

ture calculations. The linear methods deal with the full wave functions and treat all elements in the Periodic Table, i.e. s, p, d and f-electron systems [6]. Another method, the pseudopotential method, using in combination with a plane-wave basis set, has the advantage of formal simplicity. In practice it is hard to use plane waves for first-row elements or systems having d or f electrons. That's why we use pseudopotentials. Similarly, characteristics of semicore states as valence states, which is often necessary for early transition-metal elements and alkali and alkaline earth metals, are like plane wave and affects the transferability of the pseudopotential. There are several advantages of using a PSP. These are:

- The pseudopotential in the core region of the nucleus is much weaker than the true Coulomb potential.
- The obtained pseudo-wave functions in the core region are smooth and nodeless.
- The pseudopotentials and pseudo-wave functions can be efficiently described by means of a plane-wave basis set [7].

Firstly, Hamann, Schlüter and Chiang indicated and worked on Norm-Conserving (NC) pseudopotential method [5]. Their method has changed all-electron wave function (Ψ) wiht a soft nodeless pseudo wave function ($\tilde{\Psi}$) inside some core, which is very important case, because of the pseudo wave function has the same norm with all-electron wave function within the core radius, and the all-electron and pseudo are identical outside of the core radius. But there was a drawback of this method, where the transferability is adversely affected by the increase in the radius core. This problem was solved by "soft pseudopotential" formalism by Vanderbilt [8, 9]. This method is common, especially when calculation of accuracy of the 3d transition metals is important. And also this method deal with in an economical way for first row and transition metals [6, 10]. Afterwards, Car and Parrinello have improved methods and combined the density functional theory with molecular dynamics techniques [11]. The problems are solved by means of

Newton's equations. The Car-Parrinello method was first applied in the context of the plane wave pseudopotential method. They applied to the same technique for all electron methods, which deal efficiently with first row and transition metal elements and found some information about the wave function. However it is not provided by the pseudopotential approach [6, 11]. And then Blöchl pointed out the "generalized separable potentials" and he has successfully demonstrated for several interesting materials. Blöchl has further developed the Ultrasoft (US) pseudopotential concept by combining ideas from pseudopotential and Linearized Augmented Plane Wave (LAPW) methods in a conceptually elegant framework, called the Projector Augmented Wave (PAW) method [6, 12, 13]. Blöchl combined with the versatility of the LAPW method with the formal simplicity of the traditional plane-wave pseudopotential approach. The method was extended to the augmented-wave methods, such as the LAPW method and the pseudopotential method in a natural way. As an all-electron method it provides the full wave functions that are not directly accessible with the pseudopotential approach, and the potential is determined properly from the full charge densities. It demonstrates that the accuracy of the method described here compares well with the most accurate existing electronic structure methods based on the local density approximation. The quality of first principles molecular dynamics obtained with the present all-electron approach is parallel with that of state of the art Car Parrinello calculations. Hence the first energy conserving molecular-dynamics calculations based on the full wave functions are possible. Finally, it can be implemented with relatively minor effort into existing pseudopotential codes [14, 15].

The plan of the thesis is as follows; in Section 2, we give a brief overview of the concepts of pseudopotentials and pseudopotential types. Section 3 general properties of Lanthanides, review previous experimental as well as theoretical work on lattice dynamical and electronic properties of Lanthanides. Section 4 is about the calculated lattice constant, bulk modulus and their pressure derivatives. Thesis concludes with discussion and further research suggestion in Section 5. We

give figures of energy difference with respect to unit cell volume, wavefunctions and logarithmic derivatives of 4f series elements in Appendix.

CHAPTER 2

THE CONCEPT OF PSEUDOPOTENTIALS

2.1 Introduction

The concept of pseudopotential was introduced by Hellman in 1935, when it was first used in solid, then it was experimented by Herring in the 1940's [14-17]. He invented the Orthogonalized Plane Waves (OPW). The OPW method is the best approach to reduce the actual problem of an electron in a periodic potential for "nearly free" electron calculation. The theory of the pseudopotential began as an extension of the OPW method [16]. The widely use of pseudopotentials was not taken place up to the 1960's. After then, it was started to accelerate in the area of solid state physics. In the 1960's, pseudopotentials were much developed by Philips and Kleinman [18] and DFT were developed by Hohenberg and Kohn [1]. Empirical pseudo-potential was suggested by Hellman in the 1960-1970's. Norm Conserving pseudo-potential was invented by Hamann, Schluter and Chiang (HSC) in the 1980's [5]. Separable Pseudopotentials was developed by Kleinman and Bylander in the 1982. Ultrasoft pseudopotential was developed by Vanderbilt [8, 9] in the early 1990's, and optimized by Troullier and Martins (TM) [20] and Rappe, Rabe, Kaxiras and Joannopoulos (RRKJ) [21]. Projector augmented wave method was pointed out by Blöchl in the 1994 [6, 12]. After these aproaches, there are various types of pseudopotentials that are used in solid state calculations, such as empirical, norm concerving, ultrasoft, PAW. In the next section, we will review two of these pseudopotentials types, namely Troulliers Martins type norm-conserving and PAW along with its subset ultrasoft. The pseudopotential approach exploits the fact that most of the physical properties of solids are largely dependent on the valence electrons and thus the core electrons are considered to be inert. The fundamental idea of a pseudopotential is to replace

the strong Coulomb potential near to nucleus and the effects of the core electrons with a weaker ionic potential acting on the valence electrons.

2.2 Background

Scientists have wondered about structures and properties of the matters, and also how the treatment of the materials. Also, scientists have explored crystal structures of the materials which determined by development some techniques. Nowadays, whereas there are several method, one of the most commonly used is pseudopotential approximation. It has two approach to understanding the electronic structure of molecules and solids. The former description of ionic pseudopotentials is about the issue of the effect valance only electrons. This method is widely use for the ionic pseudopotentials which are more transferable in a given atom for applying to a unique ion potential. The latter method is to describe a total pseudopotentials which contains effects of the other valance electrons and it is used very common for certainly defining the bands structure, if their behaviour is predicted as adjustable empirical potentials. These methods supplied us strong insight for solids. For example, lattice constants, bulk moduli, shear moduli, cohesive energies, phonon spectra and other static and dynamical properties of solids. And also, the plane wave basis has great advantages for many calculations in the physics of solids. It provides controlled convergence and high numerical accuracy [21]. Also, atom characteristic of a pseudo is identified by means of rapid convergence in the solid.

Why do we need to generate a pseudopotential?

We need for calculation to electronic structure and material properties, and the correct behavior of the electron wavefunction (WF) in the bonding region, and also insight into features of the physics and chemistry matters. Moreover, there are several advantage of using pseudopotential. These supply a better accuracy, a different partition of electrons into valence and core, softer pseudopotential's and all-electron wavefunctions reconstruction. However, there are some disad-

vantage of using techniques which the wavefunctions are not represented the true behaviour, since the pseudo potential is derived from valanced electrons. Infact, the correct behaviour is contained by both the core electrons and the valance electrons. A pseudopotential is generated by valance electrons with nodeless pseudowavefunctions according to frozen-core approximations while electrons in the core state are extracted and the atom described. Because it is assumed that there is not contribution of bonding electrons around nucleus core, and only depend on the valance electrons. By means of this eliminating, it is described by behaviour of the atom which is only valance electrons in place of the all electrons. So, the valance electrons play an important role in bonding.

2.3 Norm-conserving pseudopotentials

Both empirical methods and the non-empirical Phillips and Kleinman approach had important limitations [18]. These restricts were solved by norm conserving approach. The description of norm-conserving potential was developed by Hamann, Schlüter and Chiang (HSC) in 1979 [5]. They proposed a method to construct non-local norm-conserving pseudopotentials to fit first-principles all-electron atomic calculations without explicitly referencing orthogonalyzation to the core states.

Norm-conserving conditions of Hamann, Schlüter and Chiang:

1. All electron and pseudo valance have the same eigenvalues in the chosen electronic configuration of the atom.

2. The pseudo-wave function is nodeless and matching with the all-electron wave function beyond a chosen core radius (r_c).

3. The integral range from 0 to r of all-electron and pseudo charge densities are the same for $\mathrm{r} > r_c$ to each valance state(norm-conservation).

4. The logarithmic derivatives of the all-electron and pseudo wavefunctions and their first energy derivatives are the same at r_c.

This method was good for s and p elements but not enough for d and f elements. Kleinman and Bylander (KB) were engaged this problem and reproduced for some elements e.g. 6s, 6p, 5d and 5f, especially 5d [22]. The configuration for d electron was better. Also wave functions were not unique and they were orthogonal in core area. This problem was handle by Kleinman and Bylander with separable form method. In an attempt to generate smoother pseudopotentials that were more suitable for an expansion in terms of plane waves which is another form of pseudopotential was introduced by Troullier and Martins [20]. The methods were generalized by Trouiller and Martins (TM) to polynomials of higher order. They were to use the additional parameters (the coefficients of the higher terms in the polynomial) to construct smoother pseudopotentials. The form of TM wavefunctions:

$\Phi_\ell(r) = r^{\ell+1} e^{p(r)}$

where $p(r) = c_0 + c_2 r^2 + c_4 r^4 + c_6 r^6 + ... + c_{12} r^{12}$

here c_n are the coefficients of p(r).

- Norm conserving conditions are the same validity here .
- The wavefunction and its first four derivatives have to be continuous at the cutoff radius, to n from 0 to 4

$$\frac{d^n \Phi}{dr^n}\Big|_{r=r_c} = \frac{d^n \Psi}{dr^n}\Big|_{r=r_c}. \tag{2.1}$$

- The pseudopotential has a zero gradient at r = 0

$$\frac{d\Phi}{dr}\Big|_{r=0} = 0. \tag{2.2}$$

This method was depended on the observation of the total energy and the kinetic energy with similar convergence properties, when extend to plane waves. This method were optimized and develop by Rappe, Rabe, Kaxiras and Joannopou-

los (RRKJ) [21]. The pseudo wavefunction of RRKJ within r_c:

$$\Phi_\ell(r) = \sum_{i=1}^{n} a_i j_\ell(q_i r) \tag{2.3}$$

where $j_\ell(q_i r)$ are the spherical Bessel functions with i - 1 zeros at positions smaller than r_c.

$$\frac{j^{'}(q_i r_c)}{j(q_i r_c)} = \frac{\Psi^{'}_\ell(r_c)}{\Psi_\ell(r_c)}. \tag{2.4}$$

- $\Phi_\ell(r)$ is normalized.
- $\Phi_\ell(r)$ has first and second derivatives continuous at r_c.
- $\Delta E_K(a_i, q_c)$ is minimal

where $\Delta E_K = -\int d^3r \Phi'_\ell \nabla^2 \Phi_\ell - \int_0^{q_c} dq q^2 |\Psi_\ell(q)|^2$.

2.4 Ultra-soft pseudopotentials

The development of first-principles norm-conserving pseudopotentials was realized by HSC [5]. This approach contains highly localized valence orbitals (e.g. for first-row and transition-metal atoms) so it is limited. Because defining the pseudo-wave-functions is difficult in a plane-wave basis [9]. The main set could be reduced to a few extent by generating optimal smoothness of the potential [21] or wave function [8] and by moving the cutoff radius outward. These approaches make up for some extent with development of Vanderbilt's new approach in 1990. Vanderbilt described construction of pseudopotentials. It has the following desirable properties:

- It contains a sum of several separable forms.
- It occurs locally and vanishes outside the core.

- The scattering properties and the derivatives of energy are true at some energies interval occupied states and also the transferiblility could be properly developed with rising number of these energies.

- The norm conserving constraint was omitted by the pseudowavefunction which could be generated by means of optimize smoothness.

- The pseudopotential itself becomes involved in the self-consistent screening process, thereby improving transferability with respect to changes in charge configuration. Together, these features allow the cutoff radius to be increased without sacrificing transferability, even for "problem" cases such as 2p and 3d orbitals [9].

In the same year, Blöchl suggested a more common type of NC for separable potentials [6, 12]. He showed that there existed an full transformation of any potential, local or nonlocal, into a separable form. In this case, the Kleinman and Bylander potential represents the first term of the resulting series expansion [22]. Even though this truncation provided often a valid and accurate approximation, in some cases the scattering properties of the atoms were not reproduced over a sufficiently wide energy range [12].

2.5 Projector Augmented-Wave Scheme

2.5.1 Formalism of Projector Augmented-Wave (PAW) functions

The projector augmented wave (PAW) method is a technique in order to solve to the electronic structure problem that reformulates the OPW method and also is defines a functional for the total energy. The PAW approach can be defined by a smooth part of a valance wavefunction like OPW approach while the norm-conservation (NC) approach is defined a smooth pseudofunction. The NC method is not as smooth as PAW method.

It is known that wave functions of real materials have fairly different properties in different regions of space. For example, although contribution of chemical bonding to the wave function is very smooth, close to the nucleus the wave function oscillates rapidly owing to the large attractive potential of the nucleus. And so valance electrons are taken into account instead of all electrons, to describe atom. Because of existing large variations in the center of atom it is hand to describe electronic structure in the core region of atom [6, 23, 24]. These difficulties is challenged by the augmented wave methods. The behavior of atom is explained by Hamiltonian equation:

$$\hat{H}|\Psi_n\rangle = \epsilon_n|\Psi_n\rangle \tag{2.5}$$

here $|\Psi_n\rangle$ is all electron wave functions. $|\Psi_n\rangle$ has needs large number of plane waves to represent atom because of rapidly oscillatory of near nuclei. Thus, we use pseudo wave functions due to they are much more smooth than all electron wave function. And also we consider a particular transformation to relevant all electron wave function with pseudo wave function. This transformation T from the pseudo wave function to the all electron wave functions, the pseudo wave functions $|\tilde{\Psi}\rangle$ and the true all electron wave functions $|\Psi\rangle$

$$|\Psi_n\rangle = \hat{T}|\tilde{\Psi}_n\rangle \tag{2.6}$$

where $\hat{T}$ is linear transform and $|\tilde{\Psi}_n\rangle$ is smooth wavefunction. We put $|\tilde{\Psi}_n\rangle$ instead of $|\Psi_n\rangle$ in the Equation[2.5]

$$\hat{H}\hat{T}|\tilde{\Psi}_n\rangle = \epsilon_n\hat{T}|\tilde{\Psi}_n\rangle. \tag{2.7}$$

We are product with linearly transformed Hamiltonian both sides of Equation[2.5]

$$\hat{T}^\dagger\hat{H}\hat{T}|\tilde{\Psi}_n\rangle = \epsilon_n\hat{T}^\dagger\hat{T}|\tilde{\Psi}_n\rangle \tag{2.8}$$

where eigenvalue of $|\Psi_n\rangle$ has similar with $|\tilde{\Psi}_n\rangle$. The aim is find $\hat{T}$ and then solve Hamiltonian equation and thus, we solve Equation[2.8]. How can we find $\hat{T}$?

We will deal with valence or semi-core electrons only because of bonding involves rearragement of those electrons only and we want to investigate binding and resulting properties. Also, the all electron wavefunctions have nodes only close to the nuclei. Wavefunctions far away from the nuclei are already smooth. So, choose $\hat{T}$ such that it acts only in a sphere of radius r_c around an atom. But, this radius is not overlap among atoms, which enough to larger between two atoms. So, choose special transformation for $\hat{T}$

$$\hat{T} = \hat{I} + \sum_a \hat{T}^a \tag{2.9}$$

where $\hat{\mathrm{T}}^a$ atom-centered contributions and here expand true wavefunction in terms of partial waves ${\phi_i}^a$. If for all-electron partial waves $|\phi_i\rangle$ have been chosen one pseudo partial wave $|\tilde{\phi}_i\rangle$, and since these waves are the identical outside of the r_c, every all-electron and pseudo waves function can be write

$$|\Psi_n\rangle = \sum_i c_i {\phi_i}^a, \tag{2.10}$$

where c_i is the same coefficient of both all-electron and pseudo wave functions, for each partial wave ${\phi_i}^a$ define a smooth partial wave $\tilde{\phi}_i^a$ [6, 23]. The local terms $\hat{\mathrm{T}}^a$ are defined with $|\phi_i\rangle$ and $|\tilde{\phi}_i\rangle$ within the chosen r_c

$$|{\phi_i}^a\rangle = (1 + \hat{\mathrm{T}}^a)|\tilde{\phi}_i^a\rangle = |\tilde{\phi}_i^a\rangle + \hat{\mathrm{T}}^a|\tilde{\phi}_i^a\rangle, \tag{2.11}$$

$$\hat{\mathrm{T}}^a|\tilde{\phi}_i^a\rangle = |{\phi_i}^a\rangle - |\tilde{\phi}_i^a\rangle. \tag{2.12}$$

And also, all-electron and pseudo waves functions have the same functions at the out of chosen cut of radius r_c

$$\tilde{\phi}_i^a(r) = \phi_i^a(r) \quad for \quad r \geq r_c \tag{2.13}$$

where r_c^a is the radius of a non overlapping sphere.

Another case, inside the augmentation sphere of atom a, we can define one-center expansions of an all-electron and pseudo state as, the smooth wavefunctions $|\tilde{\Psi}_n\rangle$

$$|\tilde{\Psi}_n\rangle = \sum_i P_{n,i}^a |\tilde{\phi}_i^a\rangle \quad for \quad r < r_c \tag{2.14}$$

where $P_{n,i}^a$ is expansion coefficients, is called projectors.

$$P_{n,i}^a = \langle \tilde{\phi}_i^a | \Psi_n \rangle = \int d\vec{r} \tilde{P}_i^a (\vec{r} - \vec{R}^a) \tilde{\Psi}_n(r) \tag{2.15}$$

where atom a is at the position $\vec{R}^a$. Each pseudo partial wave is of only one projector function and the projector functions are form

$$\sum_i |\tilde{\phi_i}^a\rangle \langle \tilde{p_i}^a| = \hat{I} \quad within \quad r_c, \tag{2.16}$$

and that the projector functions are localized inside the augmentation spheres and are orthogonal to the pseudo partial waves

$$\langle \tilde{p_{i_1}}^a | \tilde{\phi}_{i_2}^a \rangle = \delta_{i_1 i_2} \quad for \quad r < r_c. \tag{2.17}$$

We are multiply by $\langle \tilde{p_i}^a|$ both sides of Equation[2.12], and then again write

$$\hat{\mathrm{T}}^a = \sum_i (|\phi_i{}^a\rangle - |\tilde{\phi}_i^a\rangle) \langle \tilde{p_i}^a|. \tag{2.18}$$

Actually, the wave equations are solved non-relativistic Schrodinger equation or scalar-relativistic equation, however, solution to heavier elements is the best way scalar relativistic approach.

The pseudopotential is obtained by inverting the Kohn-Sham (KS) equation:

$$\Big\{ -\frac{\hbar^2}{2m}\nabla^2 + V(r) \Big\} \psi(r) = \epsilon \psi(r). \tag{2.19}$$

We write the wavefunctions in spherical coordinates

$$\psi(r) = \Big(\frac{R_{nl}(r)}{r}\Big)Y_{lm}(\hat{r}), \tag{2.20}$$

where n is quantum number, l is angular momentum and is equal to range from 0 to n-1, m is the projection of the angular momentum, which is $m = l, l-1, ...0..., -l+1, -l$.

We need to solution of Equation[2.19] Gradient and Laplacian in the spherical coordinates (r, θ, ϕ). So we write these formulas:

$$\nabla\psi = \Big(\frac{\partial\psi}{\partial r}, \frac{1}{r}\frac{\partial\psi}{\partial\theta}, \frac{1}{rsin\theta}\frac{\partial\psi}{\partial\phi}\Big), \tag{2.21}$$

$$\nabla^2\psi = \frac{1}{r}\frac{\partial^2}{\partial r^2}(r\psi) + \frac{1}{r^2 sin\theta}\frac{\partial}{\partial\theta}\Big(sin\theta\frac{\partial\psi}{\partial\theta}\Big) + \frac{1}{r^2 sin^2\theta}\frac{\partial^2\psi}{\partial\phi^2}. \tag{2.22}$$

Equation[2.20] substituted Equation[2.19]

$$\begin{aligned}\Big(-\frac{\hbar^2}{2mr}\frac{d^2R_{nl}(r)}{dr^2} + \Big(V(r)-\epsilon\Big)\frac{1}{r}R_{nl}(r)\Big)Y_{lm}(\hat{r}) \\ -\frac{\hbar^2}{2m}\Big(\frac{1}{sin\theta}\frac{\partial}{\partial\theta}\Big(sin\theta\frac{\partial Y_{lm}(\hat{r}}{\partial\theta}\Big) + \frac{1}{sin^2\theta}\frac{\partial^2 Y_{lm}\hat{r}}{\partial\phi^2}\Big)\frac{1}{r^3}R_{nl}(r) = 0\end{aligned}$$

angular part of Equation[2.23]:

$$-\frac{\hbar^2}{2m}\Big(\frac{1}{sin\theta}\frac{\partial}{\partial\theta}\Big(sin\theta\frac{\partial Y_{lm}(\hat{r}}{\partial\theta}\Big) + \frac{1}{sin^2\theta}\frac{\partial^2 Y_{lm}\hat{r}}{\partial\phi^2}\Big) = l(l+1)Y_{lm}(\hat{r})$$

radial part of Equation[2.23]:

$$-\frac{\hbar^2}{2mr}\frac{d^2R_{nl}(r)}{dr^2} + \Big(\frac{\hbar^2}{2m}\frac{l(l+1)}{r^2} + V(r) - \epsilon\Big)R_{nl}(r) = 0.$$

The (fully) relativistic KS equations are Dirac-like equations for a spinor with a large $R_{nlj}(r)$ and a small $S_{nlj}(r)$ component:

$$c\Big(\frac{d}{dr}+\frac{\kappa}{r}\Big)R_{nlj}(r)=\Big(2mc^2-V(r)+\epsilon\Big)S_{nlj}(r) \tag{2.23}$$

$$c\Big(\frac{d}{dr}+\frac{\kappa}{r}\Big)S_{nlj}(r)=\Big(V(r)+\epsilon\Big)R_{nlj}(r). \tag{2.24}$$

The full relativistic KS equations is be transformed into an equation for the large component only and averaged over spin-orbit components. In atomic units (Rydberg: $\hbar=1, m=1/2, c^2=2$):

$$\begin{aligned}-\frac{d^2R_{nl}(r)}{dr^2}+\Big(\frac{l(l+1)}{r^2}+M(r)V(r)-\epsilon\Big)R_{nl}(r)\\ -\frac{\alpha^2}{4M(r)}\frac{dV(r)}{dr}\Big(\frac{dR_{nl}(r)}{dr}+\langle\kappa\rangle\frac{R_{nl}(r)}{r}\Big)=0\end{aligned}$$

where $\alpha=1/137.036$ is the fine-structure constant, M(r) is defined as

$$M(r)=1-\frac{\alpha^2}{4}(V(r)-\epsilon). \tag{2.25}$$

The orbital angular momentum averaged value of κ is given by

$$\langle\kappa\rangle=\frac{1}{2(2+1)}(l(2l)+(-l-1))(2l+2)=-1. \tag{2.26}$$

Numerical solution of scalar-relativistic equation:

The radial (scalar-relativistic) KS equation is integrated on a radial grid. Usually logarithmic grid is taken $r_i=r_0\exp(i\Delta x)$. Thanks to this grid, we can write

$$\int_0^\infty f(r)dr=\int_0^\infty f(x)r(x)dx \tag{2.27}$$

and

$$\frac{df(r)}{dr}=\frac{1}{r}\frac{df(x)}{dx},\quad \frac{d^2f(r)}{dr^2}=-\frac{1}{r^2}\frac{df(x)}{dx}+\frac{1}{r^2}\frac{d^2f(x)}{dx^2} \tag{2.28}$$

and we write again full relativistic equation according to Equation[2.28];

$$\frac{1}{r^2}\frac{d^2R_{nl}(x)}{dx^2} = \frac{1}{r^2}\frac{dR_{nl}(x)}{dx} + \Big(\frac{l(l+1)}{r^2} + M(r)V(r) - \epsilon\Big)R_{nl}(r) - \frac{\alpha^2}{4M(r)}\frac{dV(r)}{dr}\Big(\frac{dR_{nl}(x)}{dx} + \langle\kappa\rangle\frac{R_{nl}(r)}{r}\Big)$$

we take the integral range from $r = 0$ to r_t,

$$R_{nl}(r) \simeq r^{\gamma}, \quad \gamma = \frac{l\sqrt{l^2 - \alpha^2Z^2} + (l+1)\sqrt{(l+1)^2 - \alpha^2Z^2}}{2l+1} \tag{2.29}$$

where Z is ionic charge of nucleus. In this equation, If there are a lot of nodes, then we take second integration up to the correct number of nodes due to trial eigenvalue is rise (decrease):

$$R_{nl}(r) \simeq \exp -k(r)r, \quad k(r) = \sqrt{\frac{l(l+1)}{r^2} + (V(r) - \epsilon)}. \tag{2.30}$$

Equation[2.29] and Equation[2.30] are continuously at r_t. If eigenvalue is not a correct eigenvalue, the trial eigenvector $R_{nl}(r)$ may be a peak at r_t:

$$A = \frac{dR_{nl}(r_t^+)}{dr} - \frac{dR_{nl}(r_t^-)}{dr} \neq 0 \tag{2.31}$$

as the solution we get a set of orbital energies E_i (All electron energies) and corresponding wave functions R_{nl}.

2.6 Paw Data Set

The PAW method is based on the definition of atomic spheres (augmentation regions) of r_{paw} around the atoms of system in which a base of atomic partial wave φ_i, of pseudized partial waves $\tilde{\varphi}_i$, and of projector $\tilde{p}_i$ (dual to $\tilde{\varphi}_i$) have to defined. We show wavefunctions and projector in the Fig 2.1. The core density is then deduced from the core electrons wave functions. A smooth core density

equal to the core density outside a given r_{core} matching radius (r_c), where this radius should be small enough so that for all the materials to be studied with these functions, the enclosing spheres do not overlap. On the other hand, it should be large enough so that core density $n_{core}(r)$ is well contained within r_c. A smooth partial-wave is equal to partial-waves outside for a given r_c. Pseudo partial-waves are solutions of the PAW Hamiltonian deduced from the atomic Hamiltonian by pseudizing the effective potential (a local pseudopotential is built and equal to effective potential outside a r_{vloc} matching radius). By building a compensation charge density used later in order to retrieve the total charge of the atom. This compensation charge density is located inside the PAW spheres and based on an analytical shape function (which analytic form and localization radius r_{shape}), where shape function is Sinc, Gaussian, and Besselshape. PAW data set has several important parameters, such as V_{loc}, pseudo scheme, projector-keyword, etc. Projector-keyword has three kinds. These are Blöechl, Vanderbilt and custom. In this study, we didn't use Blöechl as projector-keyword. pseudo scheme was used to generate (smooth) pseudo partial-waves, which Blöechl, Polynom, Polynom2 p q and RRKJ. We used polynom2 p q and RRKJ as pseudo scheme. V_{loc} was used to get $V_{PS}(r)$ (local) pseudopotential from all-electron effective potential $V_{eff}(r)$. V_{loc} can be used TroullierMartins, UltraSoft and Bessel. If bessel shape is chosen as shape function, localization radius (r_{shape}) is $r_{shape} = r_c * 0.8$. And if bessel is taken as V_{loc}, effective potential get $r_{vloc} = r_c * 0.7$. In all other cases, r_c equal to r_{shape}, r_{vloc} and r_{core}.

There are two relativistic approximation for used to solve atomic wave equation (non relativistic and scalar relativistic). And analytical form of the grid is determined by grid keywords (linear grid and logarithmic grid), where the number of points in the grid is 20001 if the grid is linear. On the other hand it is 2001 if the grid is logarithmic. We used scalar relativistic and logarithmic grid with 2001. Generally, choosing a scalar relativistic wave equation and a logarithmic grid (2000 points) are recommended for high Z materials and scalar-relativistic

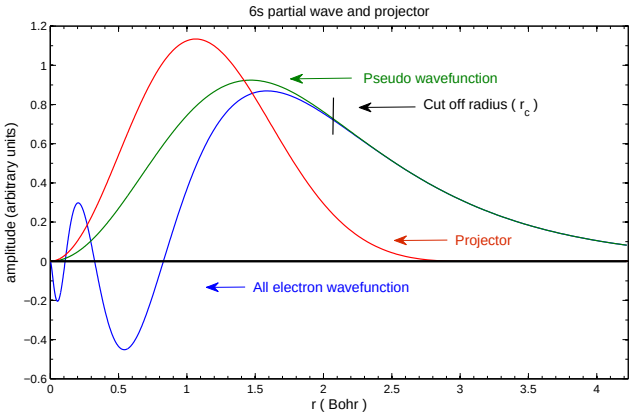

Figure 2.1: Wavefunctions and projector of La, 6s orbital

gives better results than non-relativistic.

In briefly, we need pseudopotential $V_{ps}(r)$, electron charge densities, which are pseudo charge density $\tilde{n}(r)$, core charge density $\tilde{n}_{core}(r)$, and compensation charge density $\hat{n}(r)$, projector $P^a_{n,i}$ and pseudowave functions $\tilde{\phi}^a_i(r)$ in order to solve Hamiltonian Equation. Firstly, we have generated pseudopotentials (V_{ps}). There are several ways for obtaining V_{ps} such as TroulliersMartins, Ultrasoft, and Bessel function. And also, we must choose a reference energy E_{loc}, this is generally 0 eV, and a reference angular momentum l_{loc}, which is chosen $l_{loc} = l_{max} + 1$ and this is often used for s and p elements with norm conserving scheme but sometimes it leads to problem for other elements e.g. ghost state. If we write these pseudopotentials (V_{ps}) functions:

1. TroulliersMartins type norm-conserving pseudopotential

$$\tilde{\phi}(r) = \begin{cases} r^{l_{loc}+1} \exp p(r), & r < r_c \quad ; \\ \phi(r) \qquad\qquad\quad , & r \geq r_c, \end{cases}$$

where l_{loc} is the angular momentum and $p(r)$ is even 12^{th} order polynomial

$$p(r) = \sum_{m=0}^{6} C_m r^{2m}. \tag{2.32}$$

C_m is the 7 polynomial coefficients. The screened norm-conserving pseu-

dopotential can be determined from polynomial according to

$$V_{ps}(r) = E + \frac{\hbar}{2m}\left(\frac{d^2p}{dr^2} + \left(\frac{dp}{dr}\right)^2 + \frac{2(l_{loc}+1)}{r}\frac{dp}{dr}\right). \tag{2.33}$$

2. Ultrasoft scheme without norm conservation constraint. A pseudo wave-function is written from even sixty order polynomial

$$\tilde{\phi}(r) = r^{l_{loc}+1}\sum_{m=0}^{3} C_m r^{2m}, \quad r < r_c. \tag{2.34}$$

Then, V_{PS} is deduced by inverting the wave equation.

3. Simple Bessel type pseudopotential

$$V_{ps}(r) = \alpha\frac{sin(q.r)}{r}, \quad r < r_c \tag{2.35}$$

this is zero order spherical Bessel function.

The next step to construct PAW data set is determining density equations. If these density equations are given equation form, the pseudo charge density is determined by pseudo basis functions and their occupancies $O_{n_i l_i}$:

$$\tilde{n}(r) = \sum_{n_i l_i} 0_{n_i l_i}\frac{|\tilde{\phi}_{n_i l_i}(r)|^2}{4\pi r^2}. \tag{2.36}$$

The second one is core charge density:

$$\tilde{n}_{core}(r) \equiv \begin{cases} (U_0 r^2 + U_2 r^4 + U_4 r^6)/(4\pi r^2) & for \quad r \le r_c; \\ n_{core}(r) & for \quad r \ge r_c. \end{cases}$$

where constants U_0, U_2, and U_4 are determined by r_c:

$$U_0 r_c^2 = 3d_0 - \frac{9}{8}d_1 r_c + \frac{1}{8}d_2 r_c^2 \tag{2.37}$$

$$U_2 r_c = -3d_0 + \frac{7}{4} d_1 r_c - \frac{1}{4} d_2 r_c^2 \tag{2.38}$$

$$U_4 = d_0 - \frac{5}{8} d_1 r_c + \frac{1}{8} d_2 r_c^2 \tag{2.39}$$

where $\pi r^2 \tilde{n}_{core}(r) \equiv d_0 4$ and its first two derivatives d_1 and d_2 are continuous at r_c. The last one is compensation charge density, this is defined by the total atomic charge minus the pseudo charge. This charge density can be written:

$$\hat{n}(r) = \Omega_{00} \rho_{00}(r), \tag{2.40}$$

where the monopole moment Ω_{00} is and compensation shape function is $\rho_{00}(r)$ is proportional to shape function.

$$\Omega_{00} \equiv -Z + \int d^3 r [n_{core}(r) + n(r) - \tilde{n}_{core}(r) - n_{core}(r)] \tag{2.41}$$

$$\rho_{LM}(r) \equiv N_L r^L k(r) Y_{LM}(\hat{r}) \tag{2.42}$$

here $[\sqrt{4\pi} N_L]^{-1} \equiv \int_0^{r_c} dr r^{2+2L} k(r)$ and Y_{LM} is the spherical harmonic function and N_L is normalization factor, and $k(r)$ is shape function.

Use $V_{ps}(r)$ to obtain $\tilde{\varphi}_i(r)$ and subsequently $p_i(r)$. We can choose five approaches for pseudofunctions these are Blöchl, Vanderbilt, Polynom, Polynom2 p q, and RRKJ approaches. Vanderbilt, Polynom, Polynom2 p q, and RRKJ methods are firstly use pseudowave functions and then projector obtained with the aid of these functions within framework orthogonality. There are three orthogonality functions such as Gram-Schmidt and Vanderbilt orthogonalization. Gram-Schmidt orthogonalization is explained in Blöchl pseudowave function and Vanderbilt orthogonalization is given within Vanderbilt pseudowave function.

- Blöchl: In this scheme, projectors are chosen while smooth partial waves are derived from projectors. The shapes of the functions are generally

controlled only with choice of the augmentation radius r_c and the projector functions constructed with the help of a shape function k(r) which vanishes outside the augmentation region

$$k(r) = \begin{cases} \left[\frac{\sin(\pi r/r_c)}{(\pi r/r_c)}\right]^2, r < r_c & ; \\ 0 \qquad\qquad , r \geq r_c. \end{cases}$$

The pseudo-basis functions $|\tilde{\phi}_i^0(r)\rangle$ are found by solving smooth Hamiltonian $\tilde{H}$. If we write the this equation form:

$$\left(\tilde{H}(r) - \varepsilon_i\right)|\tilde{\phi}_i^0(r)\rangle = C_i k(r)|\tilde{\phi}_i^0(r)\rangle \tag{2.43}$$

where ε_i is found by the eigenvalue of all-electron Hamiltonian Equation. After pseudo-basis functions $|\tilde{\phi}_i^0(r)\rangle$ have been determined by finding the solution of Eq.[2.43], projector functions are formed by

$$|\tilde{p}_i^0(r)\rangle \equiv \frac{k(r)|\tilde{\phi}_i^0(r)\rangle}{\langle\tilde{\phi}_i^0|k|\tilde{\phi}_i^0\rangle}. \tag{2.44}$$

We are use Gram-Schmidt orthogonalization procedure in order to found the final basis and projector functions $\{|\phi_i(r)\rangle, |\tilde{\phi}_i(r)\rangle, |\tilde{p}_i(r)\rangle\}$. The first set of basis and projector functions is given by the initial functions:

$\tilde{p}_{n_1 l}(r) \equiv \tilde{p}^0_{n_1 l}(r)$, $\tilde{\phi}_{n_1 l}(r) \equiv \tilde{\phi}^0_{n_1 l}(r)$, and $\phi_{n_1 l}(r) \equiv \phi^0_{n_1 l}(r)$ If we write a second radial basis function for that l, the final function is orthonormalized with respect to the first according to:

$$\tilde{p}_{n_2 l}(r) = \kappa_{n_2 l} \quad [\tilde{p}^0_{n_2 l}(r) - \tilde{p}_{n_1 l}(r)\langle\tilde{\phi}_{n_1 l}|\tilde{p}^0_{n_2 l}\rangle], \tag{2.45}$$

$$\tilde{\phi}_{n_2 l}(r) = \kappa_{n_2 l} \quad [\tilde{\phi}^0_{n_2 l}(r) - \tilde{\phi}_{n_1 l}(r)\langle\tilde{p}_{n_1 l}|\tilde{\phi}^0_{n_2 l}\rangle], \tag{2.46}$$

$$\phi_{n_2l}(r) = \kappa_{n_2l} \quad [\phi^0_{n_2l}(r) - \phi_{n_1l}(r)\langle\tilde{p}_{n_1l}|\tilde{\phi}^0_{n_2l}\rangle], \tag{2.47}$$

in these equations,

$$\kappa_{n_2l} \equiv \Big(1 - \langle\tilde{\phi}^0_{n_2l}|\tilde{p}_{n_1l}\rangle\Big)\langle\tilde{\phi}_{n_1l}|\tilde{p}^0_{n_2l}\rangle^{-1/2}. \tag{2.48}$$

- Vanderbilt: In this scheme, the the shape of the smooth basis functions are directly controlled, $\tilde{\phi}_i(r)$ while the projector functions $\tilde{p}_i(r)$ are derived. Each radial smooth function is chosen to have the form

$$\tilde{\phi}_{n_il_i}(r) = \begin{cases} r^{l_i+1}\sum_{m=0}^{4} C_m r^{2m}, r < r_c & ; \\ \phi_{n_il_i}(r) \qquad\qquad , r \geq r_c. \end{cases}$$

The projector functions are then formed from a linear combination of these auxiliary functions of the same angular momentum

$$\tilde{p}_{n_il_i}(r) \equiv \sum_{n_j} \chi_{n_jl_i}(r)(B^{-1})_{n_jn_i}, \tag{2.49}$$

$$\chi_{n_jl_i}(r) = \left(\varepsilon_i + \frac{\hbar^2}{2m}\Big(\frac{d^2}{dr^2} - \frac{l_i(l_i+1)}{r^2}\Big) - V^{PS}(r)\right)\tilde{\phi}_{n_il_i}(r) \tag{2.50}$$

and that the smooth basis function $\tilde{\phi}_i(r)$ is an eigenfunction of the atomic PAW Hamiltonian.

In the Eq.[2.49], the elements of the matrix B, are given by

$$B_{n_jn_i} \equiv \int_0^{r_c} dr\tilde{\phi}_{n_il_i}(r)\chi_{n_jl_i}(r). \tag{2.51}$$

For each smooth basis function, we can form a localized auxiliary function. And also Polynom and Polynom2 p q are solve similarly with Vanderbilt.

- Polynom: Use the pseudo partial waves and projector derived

$$\tilde{\varphi}_i(r) = r^{l_{loc}+1} \sum_{m=0}^{4} C_m r^{2m}. \tag{2.52}$$

- Polynom2 p q: This scheme is similar with Vanderbilt and Polynom methods and pseudowave functions are written as 2p order polynomial and then projectors derived from these pseudo functions.

$$\tilde{\varphi}_i(r) = r^{l_{loc}+1} \sum_{m=0}^{p} C_m r^{2m} \tag{2.53}$$

  where p is degree of polynomial.

- RRKJ: Use pseudowave functions with the aid of a sum of spherical Bessel functions and projectors are derived from pseudo wave functions

$$\tilde{\varphi}_i(r) = r.\Big(\alpha_1^l.j_l(q_1^l r) + \alpha_2^l, j_l(q_2^l r)\Big). \tag{2.54}$$

It is explained that the compensation charge density in charge densities section, compensation charge function has several possible types for example Sinc, Gaussian, and Bessel shape functions. We can choose one of these functions. If we write respectively these functions:

$$\rho_l(r) = Nr^l k(r) \quad with \quad k(r) = \Big[\frac{\sin(\pi r/r_c)}{(\pi r/r_c)}\Big]^2, \tag{2.55}$$

$$\rho_l(r) = Nr^l k(r) \quad with \quad k(r) = \exp(-(r/d)^2), \tag{2.56}$$

and

$$\rho_l(r) = \sum_{i=1}^{2} \alpha_i j_l(q_i r). \tag{2.57}$$

If these function are put in the Eq.[2.18], we will be find $\hat{T}$.

CHAPTER 3

4F SERIES

3.1 The General Properties of Lanthanides

When we look at under of the Periodic table, we see that there is f blocks. These blocks consist of two types f state, which are 4f and 5f blocks. 4f block is named Lanthanum or Lanthanides, which is the 6th row (4f electronic configuration) of the periodic table and their atom numbers from 57 to 71, and 5f block is called Actinium or Actinides, which is 7th row of the periodic table and also it own to 5f electronic configuration as well their atom numbers from 89 to 103. They are commonly known as rare earth elements (REEs) or rare earth metals. The their name are come from due to rarely in the earth crust.

The first of rare earth elements was discovered by J.Gadolin, who is an Archipelago Sweden, in the 1794 year [25]. Many of rare earth elements discovered by him and the name of Gadolinium came from his name. The originally, the elements were not use commercial. The firstly, to lighter flints made using the pyrophoric mischmetal were designed and produced by Karl Auer von Welsbach in the 1906. And then with the development of high-strength magnets using samarium and neodymium began to increase demand for the metals. Also they were known that their products were very hard due to strongly electropositive. By the late 1990s and early 21st century, REEs were being used in a wide variety of industries, and high tech applications, including glass polishing (cerium) and colouring (erbium and neodymium), energy storage (lanthanum), and x-ray technology (gadolinium). One of the most important applications for lanthanide metals is uses in high strength magnets. The development of samarium-cobalt and NdFeB magnets replaced electro magnets by exhibiting previously unachievable magnet energy densities. Rare earth magnets are now used in computer

hard disk drives, electric motors and magnetic resonance imaging (MRI), and also in glass production, petroleum refining, water treatment, catalysts, dyes and pigments [26, 27, 28].

Application areas of these elements are;

- lanthanum and Cerium are use in fluid catalytic cracking catalysts and high refractive index glass.
- Cerium is chemical oxidizing agents.
- Neodymium is to form ceramic capacitors.
- Gadolinium is uses in neutron capture and MRI contrasting agent.
- Thulium is product of X-ray machines.
- Europium mercury-vapor lamps and phosphors, also there is phosphors in applications of Terbium.
- Samarium, Dysprosium and Neodymium are in high strength magnets.
- Lanthanum and Lutetium for high refractive index glass.
- Many of lanthanides are use applications and products of lasers.

As a whole lanthanides are transition metals and they have 15 elements from La (57) to Lu (71). Lanthanides are common called 4f-block elements since their last electronic configurations are contained f-orbitals except for La.

The lanthanides have similar atomic structures and their chemical properties have very closely with each other, since electron exchange is only 4th state, neither 5th nor 6th states. With another the explaining, they resemble one another very closely due to the same number of electron in the outermost.

Electronic configuration of lanthanides: As the 4f and 5d electrons are too close in energy levels, they are not possible to decide whether the electron

has entered the 5d or 4f orbital. However, it is considered that the 5d orbital remains vacant and the electrons enter into the 4f orbital except for gadolinium, where the electron enters into the 5d orbital due to the presence of half filled d-orbital. At Ytterbium, all the 4f orbital's are completely filled and hence, the differentiating electron of the next element that is lutetium enters in to the 5d orbital.

Their electronic configurations are demonstrated by $[Xe]4f^{n+1}5d^{0}6s^{2}$, which $n = Z - 57$ and Z is called the atom number of element, except for La, Ce, Gd and Lu elements because La, Ce, Gd and Lu have $[Xe]4f^{n}5d^{1}6s^{2}$ configuration. For instance, Pm is of 61 electrons in nötr atom and $n = Z - 57 = 61 - 57 = 4$ $Pm = [Xe]4f^{5}5d^{0}6s^{2}$ [29, 30, 31].

Oxidation states: Lanthanides show variable oxidation states but the degree of variability is less compared to the transition elements. The most stable oxidation state of Lanthanides is of +3. In addition to the most stable +2 state, Lanthanides also show +2 and +4 oxidation states. These additional oxidations states also show stability due to presence of either half filled or completely filled or empty 4f subshell. It should be noted that the +2 and +4 oxidation states are unstable in aqueous solutions except for Ce^{+4} salts such as the ceric sulphate which acts as an oxidising agent in volumetric analysis [29].

Magnetic properties: Elements with paired electrons do not show any magnetism due to cancellation of the opposite spins due to pairing. The unpaired electrons show paramagnetic nature to some extent. Thus lanthanum and lutetium with no unpaired electrons does not show magnetism and are said to be diamagnetic in nature. The remaining members of lanthanide series are tripositive and, are paramagnetic in nature [29, 32].

3.2 Atomic Structure

It is known that elements have seven different crystal structures, however, lanthanides have three crystal structures. These are hexagonal, cubic, and rhombohedral. The hexagonals are hexagonal closed packet (hcp) and double hexagonal closed packet (dhcp). The structure of hcp elements has P3m1 symmetry and space group number 164 [27]. The hexagonal elements are Gd, Tb, Dy, Ho, Er, Tm, and Lu. The other type of hexagonal, double hexagonal elements are La, Pr, Nd, and Pm. The cubic structures have two different forms ,which are face centered cubic (fcc) and body centered cubic (bcc). The bcc is Eu. Another cubic, fcc is Ce, and Yb. The last type is rhombohedral which there is only one element (Sm), but, Sm has different crystal structure [33]. Morever, the atomic weigth of the lanthanide series increase with the rise of atomic number.This increasing is range from 138.905 to 174.967. And also they have fairly huge boiling points. Generally this temperature is about 3200^oC , but some elements are nearly 1800^oC and 2800^oC. In the general their melting point are very high, this temperature is much more than about 1200^oC.

The crystallographic and magnetic properties of the lanthanide elements exhibit striking differences as the number of 4f electrons increases. The heavy rare earths from Gd to Lu with the exception of Yb crystallize in the hexagonal close-packed (hcp) structure with the c/a ratio of approximately 1.58. The lighter rare earths with the exception of Eu crystallize in structures having more complicated stacking sequences of the hexagonal layers. The c/a ratios of the lighter sequence, when corrected for the increased stacking, are approximately 1.62 which is close to the ideal value of 1.633 [34]. The magnetic properties of the rare-earth metals are also complex. The metals which contain a partially filled 4f shell have ordering transitions as a function of decreasing temperature from a paramagnetic to an antiferromagnetic and/or a ferromagnetic state [35].

3.3 Effect of 4f Electrons on Bulk Properties

As known electronic configuration of elements affect both their physical and chemical properties such as bulk modulus, magnetic moment, chemical banding etc. And the same time, atoms are susceptible to electron numbers, which 4f electron in lanthanides plays important role in their feature, especially the numbers of f electrons in 4f series is characterized by their behaviour. For example, bulk modulus property changes with f electron, where bulk modulus are effected by rise of f electron. This change has a wide range for lanthanides, that is from 28 GPa to 48 GPa according to experimental results [36]. Similarly, our bulk results have this increase. Particularly, bulk modulus calculations of GGA in this study are very similar with effect of 4f electrons on bulk properties for experimental and theoretical results. For instance, Lanthanum (La), is the first element of Lathanides, has no any f electron which has $[Xe]4f^{0}5d^{1}6s^{2}$ electronic configuration and its bulk modulus 28 GPa, while the second elements (Ce) has only one f electron, which its $[Xe]4f^{1}5d^{1}6s^{2}$ electronic configuration and it has above 30 GPa, increase with nearly 2 GPa. These values are inharmony with experimental results [36]. In addition, the change of bulk modulus in this study is higher than experimental. In this study, bulk result of La is 28 GPa for GGA while Ce is above 38.6 GPa rise with nearly 10.6 GPa. On the other hand, the number of f electrons of Pr is of 2 electrons ($4f^{2}$) and its bulk modulu is nearly 32 GPa according to GGA calculations in this study. In generally, lanthanides have showed these properties except for Eu and Yb elements. These elements owe some decrease on bulk modulu values in contrast to other lanthanides, where these two elements are of fcc structure. Bulk modulu of Eu is from 11.7 GPa to 13.6 GPa in terms of experimental results [36-39]. Furthermore, we calculated 15 GPa for GGA and 26 GPa for LDA in this study. Another exception element (Yb) has 21.7 GPa in GGA calculation and 18 GPa in LDA calculation, and also experimental and theoretical results have a wide range 12.7 to 30.5 GPa [36, 37, 38, 41]. Unlike Eu and Yb, the others have a rise on bulk modulus by means of f electrons. In con-

clusion, we have investigated that the increase on bulk modulus values increase with atomic number in this study.

3.4 Lanthanide on Strongly-Correlated Systems

In the last decades, studies of metallic materials have related to both transition elements and rare-earth elements, especially is of 3d, 4f and 5f electronic shells and rely on their chemical compounds because such metals have a great variety of interesting phenomena and they have showed a wide range of physical properties, for example high temperature superconductors and heavy fermions. When a new material is found, its physical properties are determined by its electronic structure. Although classical band theory succeeds very well for simple metals and semiconductors due to interelectron interaction is weak, materials with d and f electron are not simply explained. Usually, these materials are called Strongly Correlated Systems (SCS) and containing transition metals, lanthanides or actinides, where the 3d or 4d electrons of the transition metals, and the 4f electrons of the lanthanides, and 5f electrons of the actinides, are localized and strongly correlated. There were a lot of model for describing SCS electronic structure problem, these approach started by Hubbard's researches in last 45 years. His method was depend on simple models such as Hubbard model, sd-model, and periodic Anderson model. The simplest models of these is Hubbard model and this is based on Hamiltonian Equaiton, such materials have been described by using the model Hamiltonian approach. Hamiltonian Equation defines electrons with spin directions $\sigma = \uparrow or \downarrow$ moving among localized states at lattice sites i and j. The electrons interact if and only if they have the same lattice site i. The Hubbard model form;

$$H = \sum_{ij,\sigma} t_{ij} c^{\dagger}_{i\sigma} c_{i\sigma} + U \Sigma_i n_{i\uparrow} n_{i\downarrow}, \tag{3.1}$$

where t_{ij} describes hopping of electrons with spin σ between orbitals at sites

i and j, and a local Coulomb interaction U between two electrons occupying the same site; $n_{i\sigma} = c^{\dagger}_{i\sigma} c_{i\sigma}$ is the density of electrons at site i with spin σ[41-45].

3.5 Previous Pseudopotentials for Lanthanides

There has been a great number of experimental and theoretical studies on physical and chemical properties of Lanthanides and their compounds [46-67], such as lattice dynamical, thermodynamic, crystal structure, elastic and electronic features. There are many ways to better understand their behaviours. For example the full potential linear muffin tin orbital (FP-LMTO) method [51], dynamical mean field theory (DMFT), the linearized muffin-tin orbital method (LMTO), the linearized augmented plane-wave (LAPW) method, full-potential linearized augmented plane-wave (FLAPW) method [52], Ashcroft's empty core (EMC) model [53], the density functional theory (DFT) [54] and ab initio pseudopotential method [55, 56]. The first study in this area was done by Lu et al. [47] in the 1989 year. They reported that band structures and electronic densities of states calculation for the bcc and fcc phases of Lanthanum and they used the general-potential LAPW method for these studies.

SUN Li et al. [48] used the first-principles plane wave method with a relativistic analytic pseudopotential of Hartwigsen, Goedcker and Hutter (HGH) scheme in the framework of local density approximation (LDA), and they reported the structural and thermodynamic properties, such as lattice constant and bulk modulus features etc., in the α phase of Cerium. Particularly, lattice constant result was agree with experimental value with error 0.3 %.

Amadon et al. [51] studied with the help of the local density approximation with a Hubbard parameter U (LDA+U) in the projector augmented wave framework in order to correctly describe to their structural parameters on the γ and β phases of cerium in the ferromagnetic and antiferromagnetic structures. Particularly, they noticed that values of U and J have an important point in LDA+U calculations but the results were not susceptible to the precise value of U and

they used $U = 6.1eV$ and $J = 0.7eV$ $(U - J = 5.4eV)$.

Later, A.B.Shick et al. [52] used the local density approximation plus Hubbard U (LDA+U) total-energy functional with the full-potential linearized augmented plane-wave method so as to calculate the electronic structure and magnetic properties of NiO and Gd. And they found very similar with previous results.

Vora [53] reported superconducting state parameters (SSP) for amorphous metals within Ashcroft's empty core (EMC) model pseudopotential framework. He worked out very well agrement with theoretical and experimental data. Chiefly, he found a strong dependency on the SSP of amorphous metals for the valence Z.

Bağcı et al. [54] studied on the structural and electronic properties in the face-centered-cubic (fcc) and double hexagonal-close-packed (dhcp) phases of lanthanum using the ab initio pseudopotential method and a generalized gradient approximation of the density functional theory and they investigated that the dhcp phase is the more stable than the fcc phase, and also, electronic band structure, electron- phonon interaction and lattice constants are calculated by them using the linear response approach. They reported that the calculations of electronic structure were very well-matched with previous theoretical studies.

Huang and Chen [56] calculated lattice dynamics for γ and α phases of Cerium e.g. the phonon band structures, bulk moduli, shear moduli, elastic constants. In this calculations, they worked with the ab initio pseudopotentials plane waves method, combined with the linear response approach. The results explained were that highly agree with experimental data.

After then, C. Hartwigsen et al [57] studied on pseudopotential parameters. They generated pseudopotential parameters of all elements up to Rn in the periodic table, which used method by separable dual-space Gaussian pseudopotentials because this method is fairly accurate due to analytic form.

Loschen et al. [58] reported the electronic structure and properties of cerium oxides (CeO_2 and Ce_2O_3) using the LDA+U and GGA (PW91)+U implemen-

tations of density functional theory and they realized that rely on selection of U parameter for these two elements in the lattice constants, bulk moduli, and density of states calculations. Also, in the calculations of CeO_2, the LDA+U results are more compatible with experimental studies than the GGA+U results. They analyzed that U value is much more susceptible in the Ce_2O_3 calculations. In generally, most of results are compatible with other studies.

Long [59] studied on some properties of RCd (R = Ce, La, Pr, Nd) such as the electronic, elastic, crystal structural, and the thermodynamic features. They used DFT within the generalized gradient approximation (GGA) for this works. The equilibrium lattice parameters in the their calculations reported similar with experimental data. Moreover, the elastic properties, the longitudinal sound velocity, transverse sound velocity, bulk modulus at zero pressure, and Debye temperature for RCd have been explored.

CHAPTER 4

PAW DATA SETS FOR LANTHANIDES

4.1 Equations of State

An Equations Of State (EOS) is the relation between functions of state, such as temperature (T), pressure (P), volume (V), internal energy or specific heat. It plays an important role for describing gases, fluids, fluid mixtures and solids. Also, Studies on equations of state (EoS) for solids have been extremely useful in the field of geophysics and condensed matter physics [68-88]. There are many uses EoS for insight into the properties of materials, such as Roy-Roy, Hama-Suito, Shanker, Stacey, Rydberg, Poirier Tarantola, Ghiroso, Kushwah, Murnaghan , Birch-Murnaghan , Cowan, Parsifar-Mason, Vinet etc. [68-88]. However,the most usely EOSs are those given by Vinet, Murnaghan, Birch-Murnaghan and Shanker. But, we use Vinet EOS in this study. We calculate equilibrium volume V_0, lattice constant, isothermal bulk modulus B_0, isothermal B_0', and magnetic moment via Vinet.

4.1.1 The Murnaghan equations of state:

The Murnaghan Equations of state is a more advanced, which was obtained by Francis D. Murnaghan (1937) [76]. This EoS is very common used, P-V data is the correct values of the room pressure bulk modulus for compressions up to about 10 % [70, 76, 77, 74]. If we write the pressure

$$P = -\Big(\frac{\partial E}{\partial V}\Big)_S \tag{4.1}$$

and the bulk modulus

$$B = -V\Big(\frac{\partial P}{\partial V}\Big)_T \tag{4.2}$$

and also the bulk modulus pressure derivative

$$B' = \Big(\frac{\partial P}{\partial V}\Big)_T \tag{4.3}$$

if we put substituted Eq.(4.2) and take integral, the result is;

$$P(V) = \frac{B_0}{B_0'}\Bigg(\Big(\frac{V_0}{V}^{B_0'}\Big) - 1\Bigg) \tag{4.4}$$

or equivalently

$$V(P) = V_0\Big(1 + B_0'\frac{P}{B_0}\Big)^{-1/B_0'}. \tag{4.5}$$

4.1.2 The Birch-Murnaghan equation of state:

The Birch-Murnaghan EoS (BMEOS) is one of the most widely used equation of state, which is a "Finite strain EoS", and s on the assumption that the strain energy of a solid undergoing compression can be expressed as a Taylor series in the finite strain [71, 78, 79, 80, 81]. The third-order Birch-Murnaghan isothermal equation of state, derived in 1947 by Francis Birch, is given by:

$$P(V) = \frac{3B_0}{2}\Bigg[\Big(\frac{V_0}{V}\Big)^{\frac{7}{3}} - \Big(\frac{V_0}{V}\Big)^{\frac{5}{3}}\Bigg]\Bigg\{1 + \frac{3}{4}\Big(B_0' - 4\Big)\Big[\Big(\frac{V_0}{V}\Big)^{\frac{2}{3}} - 1\Big]\Bigg\}. \tag{4.6}$$

Also, if we take integration of the pressure, we find the energy $\Big(\mathrm{E(V)}\Big)$:

$$E(V) = E_0 + \frac{9V_0B_0}{16}\Bigg[\Big(\frac{V_0}{V}\Big)^{\frac{2}{3}} - 1\Bigg]^3 B_0' + \Bigg[\Big(\frac{V_0}{V}\Big)^{\frac{2}{3}} - 1\Bigg]^2\Bigg[6 - 4\Big(\frac{V_0}{V}\Big)^{\frac{2}{3}}\Bigg]. \tag{4.7}$$

4.1.3 Vinet equation of state:

Due to the fact that The Birch-Murnaghan EoS do not accurately represent the volume variation of most solids under very high compression. Vinet and co-

workers (in 1986 and 1987) derived an EoS from a general inter-atomic potential. This provided as successful universal formula for solids with different types of chemical bonding up to very high compressions. For simple solids under very high compressions. The result of Vinet EoS provides a more accurate representation of the volume variation with pressure. For pressure P, isothermal bulk modulus B and pressure derivative of B, $B' = dB/dP$, the formula is written by Eq. [4.10,4.11,4.12]:

$$E(V) = E_0 + 9B_0V_0\Big(e^{A(1-x)}[A^{-1}(1-x) - A^{-2}] + A^{-2}\Big) \tag{4.8}$$

$$x = \Big(\frac{V}{V_0}\Big)^{1/3}, \quad A = \frac{3(B_0' - 1)}{2} \tag{4.9}$$

$$P = 3B_0x^{-2}(1-x)\exp\Big[\frac{3}{2}(B_0' - 1)(1-x)\Big], \tag{4.10}$$

$$B = B_0x^{-2}\Big[1 + (1-x)(1-\eta x)\exp\eta(1-x)\Big], \tag{4.11}$$

and

$$B' = \frac{1}{3}\Big[\frac{x(1-\eta) + 2\eta x^2}{1 + (\eta x + 1)(1-x)} + \eta x + 2\Big] \tag{4.12}$$

where $x = (V/V_o)^{\frac{1}{3}}$ and $\eta = \frac{3}{2}\Big[(B_0' - 1)\Big]$. Here V_0 is the volume at zero pressure, B_0 is the bulk modulus at zero pressure and the derivative of the bulk modulus is B_0' [71, 72, 73, 77, 79, 80, 81].

4.2 Lanthanum

Lanthanum (La) is the first member of the rare-earth series of elements. Its atomic number is 57 and electron configuration is $[Xe]4f^05d^16s^2$. It can exist in several phases; the double hexagonal-close-packed (dhcp) [90], hexagonal-close-packed (hcp) [91] phase and cubic phase which there is two type: the face-centered-

cubic (fcc) and the body-centered-cubic (bcc) [90, 93, 94]. Naturally formed La includes both crystalline phases. Double hexagonal-close-packed is the more stable phase for lanthanum [54]. La is the second most abundant Lanthanide after Cerium. The magnetic properties of lanthanum is paramagnetic. Its experimental magnetic moment is 0 μ_B. We have worked dhcp structure of La in the this study. Its space group number is 194 (dhcp), and its space group name is P63/mmc, and also its angles in degrees are $\alpha = \beta = 90, \gamma = 120$. This structure includes four atoms per unit cell. For the calculation of the bulk modulus properties in the dhcp phase, we evaluated the total energy as a function of lattice constant. And also, we calculated the total energy minimum around the region, the bulk modulus B_0, the pressure coefficient B_0', and equilibrium volume for dhcp La were obtained by fitting the numerical data to Vinet equation of state. The calculated equilibrium lattice parameters (a and c), bulk modulus (B_0), and the pressure derivative of the bulk modulus (B_0'), for this structure was determined at zero pressure ($P = 0$ GPa), are given in the Table 4.1.

We presented four sets of calculation with GGA (Perdew-Burke-Ernzerhof) and LDA (Perdew-Wang) exchange-correlation functionals. GGA calculation was obtained by using associated projectors as Custom, pseudo wave function as Polynom2, shape functions as Gaussian, $V_{PS}(r)$ (local) pseudopotential as UltraSoft and with parameters $r_{paw} = 2.4$ a.u. and $r_{paw} = 2.6$ a.u. configuration to generate (smooth) pseudo partial-waves. LDA calculation was obtained by using associated projectors as Custom, pseudo wave function as Polynom2, shape functions as Bessel shape, $V_{PS}(r)$ (local) pseudopotential as TroullierMartins and with parameters $r_{paw} = 2.4$ a.u. and $r_{paw} = 2.6$ a.u. configuration to generate (smooth) pseudo partial-waves. The first set used $r_{paw} = 2.6$ a.u. with GGA exchange-corelation functional. The second set used $r_{paw} = 2.4$ a.u. with GGA exchange-correlation functional. The third set has $r_{paw} = 2.6$ a.u. with LDA exchange-corelation functional while the fourth set has $r_{paw} = 2.4$ a.u. with LDA. For GGA and LDA calculations in this study, we used full optimization of

cell geometry (modify acell and rprim - normalize the vectors of rprim to generate the acell). This is the usual mode for cell shape and volume optimization. It takes into account the symmetry of the system, so that only the effectively relevant degrees of freedom are optimized. For GGA_{opt3} and LDA_{opt3} calculations used with constant-volume optimization of cell geometry (modify acell and rprim under constraint - normalize the vectors of rprim to generate the acell) [92].

In general, there were good agreement between our results and previous experimental and theoretical results. Especially, the equilibrium lattice constants were for $r_{paw} = 2.4$ a.u. and $r_{paw} = 2.6$ a.u. of GGA_{opt3}. The calculated lattice constants were lattice constant a = 3.802 Å and lattice constant c = 12.282 Å for $r_c = 2.4$ a.u. which compares well with the experimental value of lattice constant a = 3.773 Å and lattice constant c = 12.081 Å [95, 96], which computed lattice constant a and lattice constant c were larger than 0.8 % and 1.7 %, respectively. And also compares well with the theoretical value of lattice constant a = 3.801 Å and lattice constant c = 12.262 Å (GGA) [54], which calculated lattice constant a and lattice constant c were smaller than 0.03% and 0.16%. For $r_{paw} = 2.6$ a.u., the computed lattice constants were lattice constant a = 3.734 Å and lattice constant c = 12.110 Å for GGA, which was compares good with the experimental value [95, 96], and agree with theoretical value (GGA) [91]. Moreover, the computed lattice constants were lattice constant a = 3.544 Å and lattice constant c = 11.980 Å for $r_{paw} = 2.6$ a.u. of LDA was agree well with the experimental value lattice constant a = 3.772 Å and lattice constant c = 12.001 Å [36], and agree with theoretical value lattice constant a = 3.619 Å and lattice constant c = 11.677 Å (LDA) [91]. Generally, our calculated bulk modulus values were well agrement with experimental result [36], particularly both $r_{paw} = 2.4$ a.u. and $r_{paw} = 2.6$ a.u. for GGA were agree well with theoretical (GGA) [93] and experimental values [36]. For LDA, our calculated value of 33.01 GPa was 10 % higher than its theoretical value of 30.00 GPa for $r_{paw} = 2.4$ a.u., and we found 32.49 GPa for $r_{paw} = 2.6$ a.u., which was higher than 8.3 %.

Table 4.1: The lattice constants a and c ($\mathring{A}$), bulk modulus B_0 (GPa), and its pressure derivative B_0' (∂B/∂P) of dhcp La and their comparison with previous experimental and theoretical results.

	This work						Theoretical				Experimental		
	GGA	GGA_{opt3}	GGA	GGA_{opt3}	LDA	LDA	$Ref.\ [54]_{GGA}$	$Ref.\ [91]_{GGA}$	$Ref.\ [93]_{GGA}$	$Ref.\ [91]_{LDA}$	Ref. [95, 96]	Ref. [97]	Ref. [36]
r_c	2.4		2.6		2.4	2.6							
a	3.744	3.895	3.734	3.895	3.580	3.544	3.801	3.784		3.619	3.773		3.774
c	12.180	13.699	12.110	12.273	13.699	11.980	12.262	12.203		11.677	12.081		12.171
B_0	28.28	28.95	27.80	29.56	33.01	32.49	26.30	24.39	27.50	30.00		24.30	28.00
B_0'	3.02	3.15	2.96	3.34	3.52	3.42	2.89						

The another parameter B_0', we calculated 2.96 for GGA of $r_{paw} = 2.6$ a.u., which was agree well with theoretical value [GGA] [54], it was larger 2.4 %. Usually, the agreement between our and previous GGA [54, 91, 93] and LDA [91] calculations were fair well for lattice constants. As well as, there were similar results for bulk modulus, but our GGA results were quite different from theoretical value [91].

4.3 Cerium

The second element in the lanthanide series is the most abundant of these elements and is characterized chemically by having two stable valence states, III (Ce^{3+} cerous) and IV (Ce^{4+} ceric), readily accessible [90, 98]. It's atomic number is 58 and electron configuration is $[Xe]4f^15d^16s^2$, and also valence electron numbers are 3 or 4.

Generally, cerium has five distinct solid phases, i.e. a fcc α phase, Ce is tetravalent in the α' form, a fcc γ phase, and a dhcp δ phase, which is very interesting for an elemental metal [99]. The structure of cerium at atmospheric pressure and room temperature will be in the γ phase which is fcc with a lattice constant of 5.16 Å [100]. At 7 kbar cerium transforms to a phase which is also fcc with a lattice constant of 4. 85 Å [99, 100, 101] and also 4. 73 Å at 49 kbar [99]. At 55 kbar cerium changes its phase and turns into α', which is fcc with lattice constant a parameter of 4. 66 Å [100], or hcp [102] in this phase. In addition, according to [103], cerium is face-centered cubic with lattice constant a = 5.14 Å and close-packed hexagonal with lattice constant a = 3.65 Å and lattice constant c = 5.91 Å at normal room temperatures and pressures. If the pressure is raised approximately at 15.000 Atmospheres, a lattice constant a is 4.84 ±0.03 Å [103]. Moreover, there are several study from these works. Although there are five different phase of Ce, we worked γ- phase of Ce. We indicated phases of Ce in the Fig 4.1. We showed result of table all studies and experimental data in the Table 4.2.

Cerium also has magnetic and superconducting behaviors. The magnetic susceptibility follows a Curie-Weiss temperature dependence for the high-temperature γ-Ce, but it is suppressed and follows a Pauli paramagnetic temperature dependence for the low-temperature α-Ce [48].

Ce has different magnetic properties such as α phase has Pauli paramagnetism. The γ and β phases have a local moment that is antiferromagnetically ordered in the β phase, whereas the γ phase has a Curie - Weiss susceptibility [51].

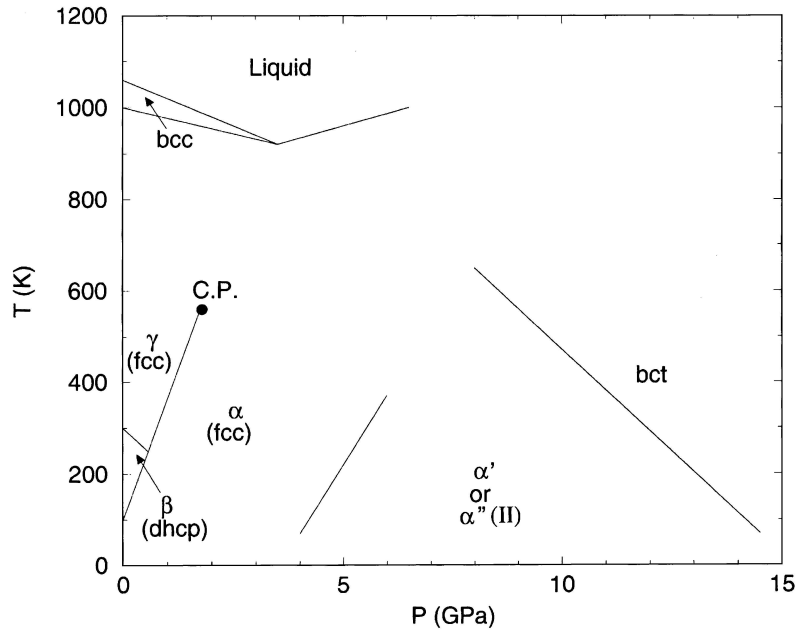

Figure 4.1: Pressure versus temperature phase diagram for cerium.

The magnetic properties of Cerium is paramagnetic. The γ phase of cerium is magnetic with a magnetic moment and susceptibility consistent with a singly occupied 4f level [99]. Its magnetic moment is 2.4 μ_B [90]. Its space group number is 225 (fcc), its space group name is Fm-3m, and also its angles are $\alpha = \beta = \gamma = 90$ in degrees.

We presented two sets of calculation with GGA (Perdew-Burke-Ernzerhof) and LDA (Perdew-Wang) exchange-correlation functionals. GGA calculation is

obtained by using associated projectors as Custom, pseudo wave function as Polynom2, shape functions as Gaussian, $V_{PS}(r)$ (local) pseudopotential as UltraSoft and with parameters $r_{paw} = 2.4$ a.u. configuration to generate (smooth) pseudo partial-waves. LDA calculation was obtained by using associated projectors as Custom, pseudo wave function as Polynom2, shape functions as Sinc, $V_{PS}(r)$ (local) pseudopotential as Bessel and with parameters $r_{paw} = 2.6$ a.u. configuration to generate (smooth) pseudo partial-waves. Although the first set uses $r_{paw} = 2.4$ a.u. with GGA exchange-correlation functional, the second set uses $r_{paw} = 2.6$ a.u. with LDA exchange-correlation functional.

Our calculation for lattice constant was 4.873 Å for GGA, which was around 5.0 % smaller than experimental values [100, 112, 106, 103]. In addition, it was agree well with theoretical values [113, 114], and it was higher 3.0 % than 4.70 Å [51]. The similar results were valid for LDA. We computed 4.801 Å, which was change around 5.0 % with experimental values and around 4-7 % with theoretical values. We calculated bulk modulus 38.64 GPa for GGA and 47.51 GPa for LDA. Our both GGA and LDA were fair different from experimental and theoretical values. For B_0' the experimental and theoretical values were not found in the literature.

Table 4.2: The lattice constants a ($\mathring{A}$), bulk modulus B_0 (GPa), and its pressure derivative B_0' (∂B/∂P) of γ-Cerium.

	This work		Experimental	Theoretical	
	GGA	LDA		GGA	LDA
a	4.874	4.801	5.160[1], 5.140[2], 5.161[12]	4.700[3], 4.690[3], 5.270[4]	4.490[3], 4.520[3], 5.200[4], 4.510[4], 4.990[4] 5.040[4], 5.120[5], 5.090[4], 5.050[4]
B_0	38.64	47.51	19.00[1], 21.00[6], 22.00[7] 24.40[8], 28.80[5], 21.50[12]	28.00[4]	30.20[9] 30.00[4], 23.90[7], 31.00[5,10] 59.00[4], 29.60[4,11], 34.00[4], 33.00[4], 31.20[5]
B_0'	5.40	5.63			

[1]Ref. [100, 112, 106] [2]Ref. [103] [3]Ref. [113, 114] [4]Ref. [51] [5]Ref. [115]
[6]Ref. [106] [7]Ref. [111] [8]Ref. [110] [9]Ref. [109] [10]Ref. [107] [11]Ref. [108] [12]Ref. [36]

We have investigated Ce in non-magnetic and ferromagnetic configuration. The results are presented in the Table 4.3.

Table 4.3: Total energy for nonmagnetic and ferromagnetic ground state (eV) of γ-Cerium.

	Non magnetic	Ferro magnetic	ΔE (E_{NM}-E_{FM})
GGA	-1067.3666	-1067.3665	$-9.2192e^{-5}$
LDA	-1072.6116	-1072.6145	0.0029

For GGA, the difference between the total energies of non-magnetic and ferromagnetic states is $-9.2192e^{-5}$ (eV) which is less than the energy resolution of our calculations. So, it is not possible to make a distinction between those states theoretically. On the other hand, since the ferromagnetic ground-state energy is lower than the energy of the non-magnetic structure for LDA, the theoretical ground state is ferro-magnetic ordered which is the experimental case, also.

4.4 Praseodymium

Praseodymium (Pr) element is the third element of lanthanides. Its atomic number is 59, and its electronic configuration is $[Xe]4f^36s^2$, and it has three or four valance electron. The crystal structure of praseodymium is double hexagonal closed packed (dhcp) and its magnetic moment is 3.60 μB [36, 90]. In addition, praseodymium is closely similar in chemical behavior with Lanthanum in most compounds.

In the Table 4.4, we indicated our computed lattice constant, bulk modulus, and its pressure derivative together with previous experimental and theoretical datas. We presented two sets of calculation with GGA (Perdew-Burke-Ernzerhof) and LDA (Perdew-Wang) exchange-correlation functionals. GGA calculation was obtained by using associated projectors as Custom, pseudo wave function as Polynom2, shape functions as Gaussian, $V_{PS}(r)$ (local) pseudopotential as UltraSoft and with parameters $r_{paw} = 2.4$ a.u. configuration to generate (smooth)

Table 4.4: The lattice constants a and c (Å), bulk modulus B_0 (GPa), and its pressure derivative B_0' (∂B/∂P) of dhcp Pr.

	This work			Experimental			Theoretical	
	GGA	GGA_{opt3}	LDA	Ref. [36]	Ref. [111]	Ref. [117]	Ref. [111]	Ref. [117]
a	3.680	3.665	3.583	3.672				
c	11.895	12.015	11.578	11.833				
B_0	32.37	27.82	33.27	28.80	30.50	29.27	34.50	41.47, 33.34
B_0'	2.97	4.94	4.79					

pseudo partial-waves. LDA calculation was obtained by using associated projectors as Custom, pseudo wave function as Polynom2, shape functions as Bessel shape, $V_{PS}(r)$ (local) pseudopotential as TroullierMartins and with parameters r_{paw} = 2.6 a.u. configuration to generate (smooth) pseudo partial-waves. Although the first set used r_{paw} = 2.4 a.u. with GGA exchange-corelation functional, the second set used r_{paw} = 2.6 a.u. with LDA exchange-correlation functional. Our calculation for lattice constants were a (3.68 Å) and lattice constant c (11.89 Å) for GGA. Calculations were fair agree well with experimental values lattice constant a (3.67 Å) and lattice constant c (11.84 Å) [145, 36] and also our lattice constant calculation for LDA was some different from GGA, which was lattice constant a (3.58 Å) and lattice constant c (11.58 Å). The estimated error was about 2.5 % for lattice constant a and about 2.2 % for lattice constant c. Furthermore, our bulk modulus results were agree with experimental value. As well as it was more agree with theoretical. Especially, our bulk modulus calculations were agree with theoretical value [117], which 32.3 GPa was error about 3 % smaller than 33.34 GPa for GGA and 33.27 GPa was around 0.2 % smaller than 33.27 GPa for LDA. Besides, there was not experimental values for B_0' in the literature.

In the ground state energetically magnetic structure calculated for NM Pr and FM Pr is showed in the Table 4.5.

Due to the fact that the ferromagnetic ground-state energy is lower than the

Table 4.5: Total energy for nonmagnetic and ferromagnetic ground state (eV) of Praseodymium.

	Non magnetic	Ferro magnetic	ΔE (E_{NM}-E_{FM})
GGA	-5192.2442	-5202.1018	9.8576
LDA	-5215.6941	-5223.9053	8.2112

energy of the non-magnetic structure, the theoretical ground state is ferromagnetically ordered which is the experimental case, as well.

4.5 Neodymium

Neodymium (Nd) is the fourth elements of 4f series and the third most abundant in the 4f series. It is obtained from the minerals bastnasite and monazite. Nowadays there is huge interest for Nd commercially due to the development of the Nd-Fe-B alloys as permanent magnet materials. And also it is common used for Nd-based lasers. Its atomic number is 60, and its electronic configuration has $[Xe]4f^4 6s^2$. Its crystal structure is double hexagonal closed packed (dhcp) [90, 36].

In this study, we used two set of exchange-correlation functionals with GGA (Perdew-Burke-Ernzerhof) and LDA (Perdew-Wang). The first set is obtained by using associated projectors as Custom, pseudo wave function as Polynom2, shape functions as Gaussian,$V_{PS}(r)$ (local) pseudopotential as UltraSoft and with parameters $r_{paw} = 2.4$ and $r_{paw} = 2.6$ a.u. configuration to generate (smooth) pseudo partial-waves. The another set was obtained by using associated projectors as Custom, pseudo wave function as Polynom2, shape functions as Bessel shape, $V_{PS}(r)$ (local) pseudopotential as TroullierMartins for parameters $r_{paw} = 2.6$ a.u. configuration to generate (smooth) pseudo partial-waves.

We investigated the lattice constants, bulk modulus, and its pressure derivative for Nd metal. We showed these studies in the Table 4.6. Our calculated lattice constants were lattice constant a (3.665 Å) and lattice constant c (11.825 Å) for $r_{paw} = 2.4$ a.u. and lattice constant a (3.639 Å) and lattice constant c (12.023

Å) for r_{paw} = 2.6 a.u. of GGA. These results were agree well with theoretical value [116] and experimental value [36]. Estimated error for lattice constant a 0.2 % and lattice constant c 0.2 % for r_{paw} = 2.4 a.u., another error for lattice constant a is 0.5 % and lattice constant c was 1.9157 % for r_{paw} = 2.6 a.u. The other calculation was GGA_{opt3} for r_{paw} = 2.4 and r_{paw} = 2.6 a.u., which are lattice constanta a 3.755 and 3.755 Å of r_{paw} = 2.4 a.u. and lattice constants c 12.101 and 12.100 Å of r_{paw} = 2.6 a.u., these were very close values. Estimated errors of these were 2.7 % for lattice constant a and 2.6 % for lattice constant c according to above 3.658 and 11.797 Å [116, 36]. The final calculation was LDA for r_{paw} = 2.6 a.u.. The result of this was constant a 3.631 Å with error 0.7 % and lattice constant c 11.605 Å with error 1.6 % [116, 36]. These lattice calculations were highly agree well with experimental and theoretical values. The other study was bulk modulus calculation. It was general similar with experimental and theoretical values. GGA, r_{paw} = 2.6 a.u. of GGA_{opt3}, and LDA were agree with experimental value, which were nearly 8 % error with experimental value, while r_{paw} = 2.4 a.u. of GGA_{opt3} was different from experimental value, which was 39.7 % smaller than experimental value. There were similar results for theoretical value, but in here errors are larger than experimental value, such as GGA for r_{paw} = 2.4 a.u. error was above 13 % [116]. In addition, there were similarities with theoretical value, for example GGA for r_{paw} = 2.6 a.u. and it was agree well theoretical value [117] with error 1.2 %. Moreover, pressure derivative of bulk modulus results GGA and LDA were agree with theoretical value [117], but GGA_{opt3} was not agree with theoretical values.

Table 4.6: The lattice constants a and c (Å), bulk modulus B_0 (GPa), and its pressure derivative B_0' (∂B/∂P) of dhcp Nd.

	This work					Experimental			Theoretical		
	GGA		GGA_{opt3}		LDA	Ref. [36]	Ref. [117]	Ref. [111]	Ref. [116]	Ref. [111]	Ref. [117]
r_c	2.4	2.6	2.4	2.6	2.6						
a	3.665	3.639	3.755	3.755	3.631	3.658			3.657		
c	11.825	12.023	12.101	12.100	11.605	11.797			11.799		
B_0	32.29	34.84	19.29	33.03	29.56	31.80	31.17	32.70	37.10	25.38	35.26, 43.44
B_0'	2.78	2.70	4.74	9.00	3.77				3.12		

We have investigated Nd in non-magnetic and ferromagnetic configurations. The results are presented in the Table 4.6 and Table 4.7, the details of the Paw data set as well as the fits to Vinet EOS are presented in the Section 4.1.3, page 34. It should be noted that for Nd the fitted equilibrium lattice parameters are highly dependent on the range of calculated volume-energy data sets. For example, if we choose the range of volumes from 883.69 to 1004.05 $(a.u.)^3$ the Vinet EOS fit gives $V_0 = 913.77$ $(a.u.)^3$, while data from V is in the range of 888.23 - 978.68 $(a.u.)^3$ the Vinet EOS gives $V_0 = 917.71$ $(a.u.)^3$ for non-magnetic GGA of $r_{paw} = 2.6$ a.u. Similarly, if we take range from 818.85 to 946.40 $(au)^3$ the equilibrium point 889.22 $(a.u.)^3$, but scale from 830.23 to 871.18 $(a.u.)^3$ would give $V_0 = 850.78$ $(a.u.)^3$ for ferromagnetic LDA of $r_{paw} = 2.6$ a.u. There is the same change for non-magnetic LDA of $r_{paw} = 2.6$ a.u. We can see these change in the Section 6, in the Figures of page 79.

Table 4.7: Total energy for nonmagnetic and ferromagnetic ground state (eV) of Neodymium.

	r_{paw}	Non magnetic	Ferro magnetic	ΔE (E_{NM}-E_{FM})
GGA	2.4	-6264.0956	-6282.8907	18.7951
GGA	2.6	-6264.3199	-6283.4869	19.1669
LDA	2.6	-6288.2099	-6289.8204	1.6106

If we look at Table 4.7, we explain nonmagnetic and ferromagnetic structures of Nd. In the Table 4.7 there is energy calculations of both GGA and LDA in the ground state, which is $r_{paw} = 2.4$ and $r_{paw} = 2.6$ a.u. In all cases for Nd, ferromagnetic type can be seen lower according to nonmagnetic results. GGA results is of highly close values in the two calculations of r_{paw} parameter.

4.6 Promethium

In our calculation for Pm calculated with GGA (Perdew-Burke-Ernzerhof) and LDA (Perdew-Wang) exchange-correlation functionals. Both GGA and LDA

Table 4.8: The lattice constants a and c (Å), bulk modulus B_0 (GPa), and its pressure derivative B_0' (∂B/∂P) of dhcp Pm.

	This work			Experimental			Theoretical
	GGA	GGA_{opt3}	LDA	Ref. [36]	Ref. [117]	Ref. [150]	Ref. [117]
a	3.630	3.736	3.606	3.650		3.650	
c	11.825	12.215	11.685	11.650		11.650	
B_0	35.06	21.26	28.05	33.00	27.89		46.07, 32.44
B_0'	3.51	4.06	3.10				

calculations of Pm were the same with calculations of Nd, radius of augmentation regions of Pm is r_{paw} = 2.4 a.u. In lattice constant calculations of GGA and LDA were high agree with experimental values. Our lattice constant calculation calculated 3.630 Å for lattice constant a with error 0.6 % and 11.825 Å for lattice constant c with error 1.5 %. For LDA, we calculated 3.606 Å for lattice constant a with error 1.2 % and 11.685 Å for lattice constant c with error 0.3 %. GGA_{opt3} was lattice constant a 3.736 and lattice constant c 12.215 Å, which were estimated errors 2.4 % and 4.9 % [150, 36]. Bulk modulus calculation of GGA was agree with experimental [36] and theoretical values [117], but was not agree with experimental value [117]. LDA was only agree with experimental value [117], which was not agree with the others. On the other hand, GGA_{opt3} was not agree with anything. Also, we calculated pressure derivative of bulk, which was 3.51 for GGA, 4.06 for GGA_{opt3}, and 3.10 for LDA which was not experimental values for B_0'.

Table 4.9: Total energy for nonmagnetic and ferromagnetic ground state (eV) of Promethium.

	Non magnetic	Ferro magnetic	ΔE (E_{NM}-E_{FM})
GGA	-7493.8718	-7517.6992	23.8274
LDA	-7522.7562	-7543.4695	20.7134

Pm is interesting and important point in our studies. Pm is more different than above 20 eV, between nonmagnetic and ferromagnetic in the ground state. In contrast to the other elements, only Pm has this different and theoretical ground state is ferromagnetic which is the experimental case, as well.

4.7 Samarium

Samarium (Sm) element is made straight from the oxide by reaction with lanthanum. Its structure is uncommon complex in the room temperature since contain of the f-orbitals in the bonding [90]. In generally, there are three phase, which are rhombohedral, cubic and hexagonal. But we used rhombohedral structure of it with the space group $R\bar{3}m$. For rhombohedral structure; a = 8.996 Å, and $\alpha = 23^{\circ}13^{'}$ [137]. Its atomic number is 62 and its electronic configuration has $[Xe]4f^{6}6s^{2}$.

Table 4.10: The lattice constants a ($\mathring{A}$), bulk modulus B_0 (GPa), and its pressure derivative B_0' (∂B/∂P) of Rhombohedral Sm.

	This work			Experimental	
	GGA		LDA	Ref. [137]	Ref. [36]
r_{paw}	2.4	2.6	2.4		
a	9.120	9.120	8.999	8.996	
B_0	32.31	30.79	27.16		37.8
B_0'	8.99	7.67	5.76		

We calculated for three kind of exchange-correlation functionals, GGA (Perdew-Burke-Ernzerhof) and LDA (Perdew-Wang) exchange-correlation functionals. GGA was obtained by using associated projectors as Custom, pseudo wave function as Polynom2, shape functions as Gaussian, $V_{PS}(r)$ (local) pseudopotential as UltraSoft at both $r_{paw} = 2.4$ a.u. and $r_{paw} = 2.6$ a.u. to generate (smooth) pseudo partial-waves. LDA was obtained by using associated projectors

as Custom, pseudo wave function as Polynom2, shape functions as Bessel shape, $V_{PS}(r)$ (local) pseudopotential as TroullierMartins at $r_{paw} = 2.6$ a.u. to generate (smooth) pseudo partial-waves.

Our lattice calculations of GGA to two r_{paw} were high agree with experimental value [137]. We found 4.826 Å with error 1.3 % according to 4.760 Å [137]. Another lattice constant result was more agree with experimental value [137] and it had 4.762 Å with error % 0.03. The lattice constant results both GGA and LDA of Sm had very close to experimental value. Although GGA of bulk modulus was agree with experimental value, LDA of bulk modulus was distant to experimental value. GGA found 32.31 GPa with error 14.5 % [36] for $r_{paw} = 2.4$ a.u. and 30.79 GPa with error 18.6 % [36], but LDA was not similar with GGA since it found 27.16GPa with error 28.2 % [36]. Estimated error of LDA was different from GGA and it had high distant to experimental value [36].

Table 4.11: Total energy for nonmagnetic and ferromagnetic ground state (eV) of Samarium

	r_{paw}	Non magnetic	Ferro magnetic	ΔE (E_{NM}-E_{FM})
GGA	2.4	-6668.2715	-6678.9689	10.6974
GGA	2.6	-6671.6527	-6679.5909	7.9382
LDA	2.4	-6689.6126	-6706.4919	16.8793

Sm has close results to two r_{paw} values of ferromagnetic in the GGA studies, and these results can be seen easily in the Table 4.11. And also, ferromagnetic in the three calculations is lower than nonmagnetic. In addition, the theoretical ground state of ferromagnetic results are similar with experimental case.

4.8 Europium

Europium (Eu) has 63 atomic number and $[Xe]4f^7 6s^2$ electronic configuration. Its structure is body centered cubic (bcc) [36].

For GGA calculation of Eu was obtained by using associated projectors as Custom, pseudo wave function as Polynom2, shape functions as Gaussian,

Table 4.12: The lattice constants a and c (Å), bulk modulus B_0 (GPa), and its pressure derivative B_0' (∂B/∂P) of bcc Eu.

	This work		Experimental			Theoretical		
	GGA	LDA	Ref. [36]	Ref. [150]	Ref. [37]	Ref. [38]	Ref. [39]	Ref. [40]
a	5.585	4.698	4.583	4.583	4.130			
B_0	14.89	25.99	8.30		11.70	13.6	11.80	12.4
B_0'	2.91	3.19			3.00	3.00	1.80	2.80

Ref. [37] is pressure in the 5.9 GPa.

$V_{PS}(r)$ (local) pseudopotential as Ultrasoft and with parameters $r_{paw} = 2.6$ a.u. configuration to generate (smooth) pseudo partial-waves. On the other hand, for LDA calculation was obtained by using associated projectors as Custom, pseudo wave function as Polynom2, shape functions as Bessel shape, $V_{PS}(r)$ (local) pseudopotential as TroullierMartins for parameters $r_{paw} = 2.4$ a.u. configuration to generate (smooth) pseudo partial-waves. There were two lattice constant calculations for Eu metal, which were GGA and LDA calculations. Though LDA calculation was 4.698 Å and agree with experimental value (4.583 Å) [36], GGA result was disagree. Also, LDA was distant to experimental value (4.130 Å) [37]. The other calculation was bulk modulus calculation. Unlike GGA computation, which was 14.89 GPa with error 9.4 %, was comply to theoretical value [38], it was disagree with experimental and the other theoretical values. In contrast to GGA result, LDA was agree neither experimental nor theoretical values. B_0' computation of GGA was well agree with experimental and theoretical values except for theoretical value [39]. As well as, LDA result was resemble by experimental [37] and theoretical values [38]. Yet, it was distinct from theoretical values [39, 40].

Owing the fact that the ferromagnetic ground-state energy is less than the energy of the non-magnetic structure, the theoretical ground state is ferro-magnetically ordered which is the experimental case, also.

Table 4.13: Total energy for nonmagnetic and ferromagnetic ground state (eV) of Europium

	Non magnetic	Ferro magnetic	ΔE (E_{NM}-E_{FM})
GGA	-2614.4384	-2620.0711	5.6328
LDA	-2617.8074	-2618.3075	0.5002

4.9 Gadolinium

The atomic number of gadolinium is 64 and it has electronic configuration $[Xe]4f^7 5d^1 6s^2$. It has different atomic structures, namely the hcp, dhcp, and fcc structures [121]. But, we have used hcp structure of Gd metal in this study. It has hcp structured at the room temperature [123]. It has been reported that it is in ferromagnetic structure at the Curie point of 16 °C [124, 125, 134]. Gd^{3+} ion has the stable $4f^7$ configuration and, with seven unpaired electrons, a high magnetic moment; many uses depend on Gd's magnetic properties. Nowadays, it is widely used, for example, in medicine due to magnetic resonance imaging.

The calculation of Gd was different from previous calculations. It was obtained by using associated projectors as Custom, pseudo wave function as RRKJ, shape functions as Gaussian, $V_{PS}(r)$ (local) pseudopotential as TroullierMartins and with parameters $r_{paw} = 2.6$ a.u. configuration to generate (smooth) pseudo partial-waves of GGA calculation. Also LDA calculation was obtained by using associated projectors as Custom, pseudo wave function as Polynom2, shape functions as Sinc shape, $V_{PS}(r)$ (local) pseudopotential as Bessel for parameters $r_{paw} = 2.4$ a.u. configuration to generate (smooth) pseudo partial-waves.

Table 4.14: The lattice constants a and c (Å), bulk modulus B_0 (GPa), and its pressure derivative B_0' (∂B/∂P) of hcp Gd.

	This work			Experimental					Theoretical			
	GGA	GGA_{opt3}	LDA	Ref. [36]	Ref. [37]	Ref. [126]	Ref. [127]	Ref. [130]	Ref. [41]	Ref. [129]	Ref. [131]	Ref. [132]
a	3.609	3.635	3.519	3.634	3.580	3.629						
c	5.699	5.708	5.636	5.781	5.695	5.796						
B_0	32.91	29.05	42.69	37.90	34.00		41.30	39.90	39.0	38.80	35.0, 40.9	45.3, 41.0
B_0'	3.17	2.32	3.35		3.20							

Ref. [37] is the pressure 1.4 GPa
Ref. [126] is the temperature 106 °K.

In this study, our lattice constant calculations were close resemble with all experimental values. For instance, GGA_{opt3} was computed 3.635 and 5.708 Å with error 0.02 % for lattice constant a and error 1.3 % for lattice constant c with respect to experimental value [36]. In addition, GGA was calculated 3.609 and 5.699 Å, which was 0.8 % more than experimental value 3.580 Å for lattice constant a and 0.1 % more than experimental value 5.695 Å for lattice constant c [37]. Similarly, LDA was lattice constant a 3.519 Å with 1.7 % error and lattice constant c 5.636 Å with 1.0 % error compare by experimental value [37]. The other calculation was bulk modulus calculation. Bulk modulus calculation of GGA was 32.91 GPa and was agree with experimental value 34.00 GPa (3.2 % error) [37] and theoretical value 35.00 GPa (5.9 % error) [131], but it is not similar with experimental values such as 41.30 GPa [128] and 39.90 GPa [130] and theoretical value e.g. 38.80 GPa [129]. Even though GGA was agree some experimental and theoretical values, GGA_{opt3} and LDA were not identical to none experimental and theoretical values. Moreover, pressure derivative of bulk modulus of GGA and LDA were related with experimental value [37]. Especially, GGA was 3.17 GPa with 0.9 % less than experimental value 3.20 GPa, was closely resemble. As well, LDA was uniform with 4.9 % error. However, GGA_{opt3} was not association with experimental value and its error was 27.5 % less than experimental value.

Table 4.15: Total energy for nonmagnetic and ferromagnetic ground state (eV) of Gadolinium

	Non magnetic	Ferro magnetic	ΔE (E_{NM}-E_{FM})
GGA	-6103.4327	-6119.3319	15.8992
LDA	-6119.1536	-6.1406339	21.4804

Since the ferromagnetic ground-state energy is lower than the energy of the non-magnetic structure, the theoretical ground state is ferro-magnetically ordered which is the experimental case, as well.

4.10 Terbium

Terbium (Tb) metal has electronic configuration $[Xe]4f^9 6s^2$, with 65 atomic number. It has a hexagonal structure and orthorhombic (ortho), we used hcp structure for this calculation, also there is two phase transitions of Tb, which is from paramagnetism to a helical spin structure at the range of $223.3 - 231\,^{\circ}$K and from the helical spin structure to a ferromagnetic state in the range of $210 - 220\,^{\circ}$K [118].

Table 4.16: The lattice constants a and c (Å), bulk modulus B_0 (GPa), and its pressure derivative B_0' (∂B/∂P) of hcp Tb.

	This work			Experimental			
	GGA	GGA_{opt3}	LDA	Ref. [36]	Ref. [150]	Ref. [119]	Ref. [120]
a	3.572	3.635	3.498	3.606	3.606	3.599	3.601
c	5.820	5.708	5.672	5.697	5.697	5.696	5.694
B_0	31.40	39.96	35.17	38.70			
B_0'	2.99	2.45	3.70				

Ref. [119] and Ref. [120] are the lattice parameters for Tb at room temperature.

We introduced two sets of calculation with GGA (Perdew-Burke-Ernzerhof) and LDA (Perdew-Wang) exchange-correlation functionals for Tb. GGA calculation was obtained by using associated projectors as Custom, pseudo wave function as RRKJ, shape functions as Gaussian, $V_{PS}(r)$ (local) pseudopotential as Bessel to generate (smooth) pseudo partial-waves. LDA calculation was obtained by using associated projectors as Custom, pseudo wave function as Polynom2, shape functions as Bessel shape, $V_{PS}(r)$ (local) pseudopotential as TroullierMartins to generate (smooth) pseudo partial-waves. Although the first set used $r_{paw} = 2.4$ a.u. with GGA exchange-correlation functional, the second set used $r_{paw} = 2.6$ a.u. with LDA exchange-correlation functional. The lattice

constant calculations of all calculations of Tb were agree well with all experimental values [119, 120, 150, 36]. Bulk modulus calculation of GGA_{opt3} and LDA were agree with experimental value, which was 39.96 GPa with estimated error 3.3 % for GGA_{opt3} and 35.17 GPa with estimated error 9.1 %. Bulk modulus calculation of GGA was calculated 31.40 GPa larger than experimental value with error 18.9 %. For Tb, we didn't find experimental value in the literature.

Table 4.17: Total energy for nonmagnetic and ferromagnetic ground state (eV) of Terbium

	Non magnetic	Ferro magnetic	ΔE (E_{NM}-E_{FM})
GGA	-7074.8458	-7088.0366	13.1908
LDA	-7090.5470	-7104.0365	13.4895

Due to the fact that the non-magnetic ground-state energy is higher than the energy of the ferromagnetic structure, the magnetic type of Tb in the ground state is ferro-magnetically ordered the same as experimental value, also.

4.11 Dysprosium

The atomic number of Dysprosium (Dy) metal is 65 and has electronic configuration $[Xe]4f^{10}6s^2$. The chemical properties of Dy are high similar with Yttrium, these two metals having trivalent ions of very resemble size. It has a very high magnetic moment of above 10.6 Bohr magnetons in order to strong spin-orbit coupling. Dysprosium exhibits a magnetic anomaly at about 175 °K and a ferromagnetic Curie point near 90 °K [126, 135, 136]. There are two crystal structure of its, which hcp [123] and ortho [36].

We offered two type of exchange-correlation functionals, GGA (Perdew-Burke-Ernzerhof) and LDA (Perdew-Wang) exchange-correlation functionals. The first of them was obtained by using associated projectors as Custom, pseudo wave function as Polynom2, shape functions as Gaussian, $V_{PS}(r)$ (local) pseudopotential as UltraSoft to generate (smooth) pseudo partial-waves. The latter was

Table 4.18: The lattice constants a and c (Å), bulk modulus B_0 (GPa), and its pressure derivative B_0' (∂B/∂P) of hcp Dy.

	This work			Experimental		
	GGA	GGA_{opt3}	LDA	Ref. [36]	Ref. [150]	Ref. [126]
a	3.486	3.425	3.635	3.592	3.592	3.584
c	5.843	5.760	5.708	5.650	5.650	5.668
B_0	42.39	46.06	41.93	40.50		
B_0'	2.74	3.70	2.31			

Ref. [126] is the temperature $48 - 50\,^{\circ}$K

obtained by using associated projectors as Custom, pseudo wave function as Polynom2, shape functions as Bessel shape, $V_{PS}(r)$ (local) pseudopotential as Bessel to generate (smooth) pseudo partial-waves. Both GGA and LDA calculations had same $r_{paw} = 2.4$ a.u.

Our all lattice constant results were agree well with experimental values [126, 150, 36]. Estimate error of them were smaller than error 5.0 %. GGA is lattice constant a 3.486 Å with error 2.9 % and lattice constant c 5.843 Å with error 3.4 %. GGA_{opt3} was lattice constant a 3.425 Å with 4.7 % and lattice constant c 5.760 Å with 2.0 %. LDA was lattice constant a 3.635 Å with 1.197 % and lattice constant c 5.708 Å with 1.0 %. Bulk modulus results of GGA and LDA were similar with experimental value [36], we found 42.39 GPa which was larger 4.7 % than experimental value 40.50 GPa for GGA and 41.93 GPa was larger 3.5 % than experimental value 40.50 GPa for LDA. However, GGA_{opt3} was 46.06 GPa and it was not similar with experimental value, it estimated error 13.7 %. For B_0' no experimental value was found.

As the non-magnetic ground-state energy, which is above 16 eV for GGA and nearly 11.4 eV for LDA is higher than the energy of the ferromagnetic structure, Dy in the theoretical ground state is of ferro-magnetically ordered, and also it is

Table 4.19: Total energy for nonmagnetic and ferromagnetic ground state (eV) of Dysprosium

	Non magnetic	Ferro magnetic	ΔE (E_{NM}-E_{FM})
GGA	-8137.3726	-8153.4685	16.0959
LDA	-8161.5075	-8172.9268	11.4193

the experimental case.

4.12 Holmium

Holmium is one of the least abundant lanthanides with atomic number 67 and electronic configuration $[Xe]4f^{11}6s^2$ Holmium metal has the highest magnetic moment $\approx 10\mu_B$ (per atom) below the Neel temperature $T_N \approx 131\,^{\circ}$K [138] and its crystal structure hcp [141]. It show ferromagnetic property at low temperature.

Table 4.20: The lattice constants a and c (Å), bulk modulus B_0 (GPa), and its pressure derivative B_0' (∂B/∂P) of hcp Ho.

	This work			Experimental		
	GGA	GGA_{opt3}	LDA	Ref. [36]	Ref. [150]	Ref. [139]
a	3.445	3.635	3.344	3.578	3.578	3. 577
c	5.874	5.708	5.768	5.618	5.618	5. 616
B_0	41.84	41.49	48.25	40.20		
B_0'	1.98	4.14	2.31			

Ref. [139] is the lattice parameters at room temperature.
Ref. [140] is magnetic moment at the 4.2 °K.

GGA calculation of Ho was identical with Gd calculation, but $r_{paw} = 2.4$ a.u. was different from $r_{paw} = 2.6$ a.u. of Gd. Not only LDA calculationt of Ho was similarly, but also $r_{paw} = 2.4$ a.u. of Ho was similar with Gd. The lattice constant calculations of Holmium metal were general agree with experimental

values [139, 150, 36]. Particularly, GGA_{opt3} calculation was close resemble with experimental value, computed lattice constant a 3.635 and lattice constant c 5.708 Å were 1.6 % and 1.6 % larger than experimental lattice constant a 3.578 and lattice constant c 5.618 Å. GGA estimated error 3.7 % for lattice constant a and 4.6 % for lattice constant c. The lattice constants of LDA were lattice constant a 3.344 and lattice constant c 5.768 Å with error 6.5 % and 2.7 %. Whereas bulk modulus calculation of GGA and GGA_{opt3} were similar with experimental value, LDA was disagree. The bulk modulus result of GGA was 41.84 GPa, and it was 4.1 % larger than experimental value 40.20 GPa. Similarly, GGA_{opt3} was investigated 41.49 GPa with error 3.2 % . By contrast with of these, LDA was computed 48.25 GPa and was 20.0 % error. For Ho no information was found about B_0' in the literature.

Table 4.21: Total energy for nonmagnetic and ferromagnetic ground state (eV) of Holmium

	Non magnetic	Ferro magnetic	ΔE (E_{NM}-E_{FM})
GGA	-9307.2816	-9322.7882	15.5067
LDA	-9332.9622	-9343.1239	10.1617

When we can see the Table 4.21, the ferromagnetic ground-state energy is lower than the energy of the non-magnetic structure. Thus the theoretical ground state is ferro-magnetically ordered similar to the experimental result.

4.13 Erbium

Erbium has configuration $[Xe]4f^{12}6s^2$ with atomic number 68. The chemical treatment of Er^{3+} ion is similar with Yttrium. The structure of erbium metal has hexagonal, close-packed for all exposures [123].

GGA calculation of Er was similar with GGA calculation of La, and LDA calculation was similar with LDA calculation of Ce. Our lattice constant calculations were agree with experimental value for Er. All of them have smaller error than 2.0 %. For example, LDA was lattice constant a 3.556 Å, which is 0.1 %

Table 4.22: The lattice constants a and c (Å), bulk modulus B_0 (GPa), and its pressure derivative B_0' (∂B/∂P) of hcp Er.

	This work			Experimental		
	GGA	GGA_{opt3}	LDA	Ref. [36]	Ref. [150]	Ref. [126]
a	3.476	3.635	3.556	3.559	3.559	3.558
c	5.626	5.708	5.673	5.585	5.585	5.590
B_0	38.48	29.89	22.39	44.40		
B_0'	2.53	1.16	4.73			

Ref. [126] is at the temperature $42.5 - 43.5\,^{\circ}$K

smaller than experimental value 3.559 Å and lattice constant c 5.673 Å, which was 1.6 % larger than experimental value 5.585 Å [126, 150, 36]. Bulk modulus calculations were usual distant to experimental value. GGA calculation was 38.48 GPa and 13.3 % smaller than experimental value 44.40 GPa [36]. GGA_{opt3} and LDA were highly different from experimental bulk modulus value.

We demonstrated the total energy for nonmagnetic and ferromagnetic ground state (eV) of Erbium in the Table 4.23. On account of the fact that the ferromagnetic ground-state energy is lower than the energy of the non-magnetic structure. So, the theoretical ground state is ferro-magnetic. Moreover, experimental case is the ferro-magnetically ordered.

Table 4.23: Total energy for nonmagnetic and ferromagnetic ground state (eV) of Erbium

	Non magnetic	Ferro magnetic	ΔE (E_{NM}-E_{FM})
GGA	-10589.4764	-10596.7659	7.2895
LDA	-10609.8056	-10618.9475	9.1419

4.14 Thulium

Thulium, the rarest of the "abundant earths", is atomic number 69 and has $[Xe]4f^{13}6s^2$ configuration. Thulium is the last magnetic element of rare earth metal series. Its crystal structure is hcp and its magnetic structure has both paramagnetic and ferromagnetic structures [142].

Table 4.24: The lattice constants a and c (Å), bulk modulus B_0 (GPa), and its pressure derivative B_0' (∂B/∂P) of hcp Tm.

	This work			Experimental				Theoretical
	GGA	LDA	GGA_{opt3}	Ref. [36]	Ref. [150]	Ref. [117]	Ref. [143]	Ref. [117]
a	3.590	3.445	3.635	3.538	3.538		3.537	
c	5.885	5.562	5.708	5.554	5.554		5.504	
B_0	22.04	34.27	45.39	44.50		40.44		57.71, 69.07
B_0'	6.78	4.55	$3.42e^{-12}$					

GGA calculation of Tm was obtained by using associated projectors as Custom, pseudo wave function as Polynom2, shape functions as Gaussian, $V_{PS}(r)$ (local) pseudopotential as UltraSoft and with parameters $r_{paw} = 2.6$ a.u. configuration to generate (smooth) pseudo partial-waves. LDA calculation of Tm was obtained by using associated projectors as Custom, pseudo wave function as Polynom2, shape functions as Bessel shape, $V_{PS}(r)$ (local) pseudopotential as TroullierMartins and with parameters $r_{paw} = 2.4$ a.u. configuration to generate (smooth) pseudo partial-waves. Although the first set used $r_{paw} = 2.6$ a.u. with GGA exchange-corelation functional, the second set used $r_{paw} = 2.4$ a.u. with LDA exchange-correlation functional.

In general, our lattice constant calculations for Tm metal were similar with experimental value. Especially, LDA and GGA_{opt3} results were agree with experimental value [150]. For LDA lattice constant a 3.445 and lattice constant c 5.562 Å were computed and estimated error with 2.6 % less than experimental value 3.538 Å for lattice constant a and was 0.2 % more than experimental value 5.554 Å for lattice constant c. GGA_{opt3} was computed lattice constant a 3.635 Å

with error 2.7 % and lattice constant c 5.708 Å with error 2.8 % . Furthermore, GGA calculation found lattice constant a 3.590 (1.5 % error) and lattice constant c 5.885 Å (6.0 % error). Otherwise, bulk modulus calculations were some different from experimental and theoretical values. Only GGA_{opt3} was fair agree with experimental value [36]. Its compute was 45.39 GPa and was larger about 2.0 % than experimental value 44.50 GPa. It was distinct to others experimental value [117] and theoretical value [117]. GGA and LDA bulk modulus calculations were extreme distant to experimental and theoretical values. Our computed were 22.04 GPa for GGA and 34.27 GPa for LDA, whereas experimental values are 40.44 GPa [117] and 44.50 GPa [36] and also theoretical values were 57.71 and 69.07 GPa [117].

Table 4.25: Total energy for nonmagnetic and ferromagnetic ground state (eV) of Thulium

	Non magnetic	Ferro magnetic	ΔE (E_{NM}-E_{FM})
GGA	-11980.2582	-11981.0079	0.7497
LDA	-12003.3041	-12007.5292	4.2251

4.15 Ytterbium

In chemical behavior this element resembles Yttrium and the heavy lanthanides. It has $[Xe]4f^{14}6s^2$ electron configuration. There is the three crystal structures of ytterbium, hcp ($\alpha - Yb$) , fcc ($\beta - Yb$) and bcc, which are depending upon the temperature and pressure [146, 147]. We present the results from a first-principles study of the crystal structure of the three close-packed polymorphs of ytterbium, bcc($\gamma - Yb$), fcc ($\beta - Yb$) and hcp ($\alpha - Yb$).

We calculated for two kind of exchange-correlation functionals, GGA (Perdew-Burke-Ernzerhof) and LDA (Perdew-Wang) exchange-correlation functionals. GGA was obtained by using associated projectors as Custom, pseudo wave function as Polynom2, shape functions as Gaussian, $V_{PS}(r)$ (local) pseudopotential as UltraSoft to generate (smooth) pseudo partial-waves. LDA was obtained by using

Table 4.26: The lattice constants a and c (Å), bulk modulus B_0 (GPa), and its pressure derivative B_0' (∂B/∂P) of bcc Yb.

	This work		Experimental			Theoretical		
	GGA	LDA	Ref. [36]	Ref. [150]	Ref. [37]	Ref. [41]	Ref. [38]	Ref. [146]
a	5.133	5.107	5.485	5.485	5.415			5.041[1], 5.295[2], 5.281[3]
B_0	21.75	18.87	30.50		14.00	12.70	14.00	
B_0'	4.25	3.66			3.20		3.60	

Ref. [37] is pressure in the 0.5 GPa
[1] LDA/SVWN
[2] GGA/PBE
[3] GGA/PW91

associated projectors as Custom, pseudo wave function as Polynom2, shape functions as Sinc shape, $V_{PS}(r)$ (local) pseudopotential as Bessel to generate (smooth) pseudo partial-waves. Both GGA and LDA calculations were same $r_{paw} = 2.4$ a.u.

In lattice constant calculations of our study for bcc Yb was agree well with both experimental value [37, 150] and theoretical value [146]. The theoretical value was more closer than experimental value. We were investigated 5.133 Å for GGA, which was about 5-6 % more than experimental value and nearly error 2-3 % compared to theoretical value of this study, and 5.107 Å for LDA, which was given same result with GGA. On the other hand, we calculated 21.75 GPa for GGA and 18.87 GPa for LDA, which were disagree not only experimental values [37, 36] but also theoretical values [41, 38]. Bulk modulus derivative of GGA was distant to experimental value [37] and theoretical value [38]. Although LDA was not resemble by experimental, it was similar theoretical with error 1.7 %.

Table 4.27: Total energy for nonmagnetic and ferromagnetic ground state (eV) of Ytterbium

	Non magnetic	Ferro magnetic	ΔE (E_{NM}-E_{FM})
GGA	-6744.4371	-6744.4371	$-1.0885e^{-6}$
LDA	-6756.5984	-6756.5983	$-1.3606e^{-6}$

The difference between the total energies of non-magnetic and ferromagnetic states is $-1.0885e^{-6}$ (eV) for GGA and $-1.3606e^{-6}$ (eV) for LDA, which is less than the energy resolution of our calculations. Hence, it is impossible to make a distinction between those states theoretically.

4.16 Lutetium

The last member of the Lanthanide series is, along with thulium, the least abundant. Lutetium has a full 4f electron shell, and so magnetic moment of this metal is absence. Its crystal structure is hcp.

Table 4.28: The lattice constants a and c (Å), bulk modulus B_0 (GPa), and its pressure derivative B_0' (∂B/∂P) of hcp Lu.

	This work			Experimental			Theoretical	
	GGA	GGA_{opt3}	LDA	Ref. [36]	Ref. [150]	Ref. [149]	Ref. [41]	Ref. [148]
a	3.363	3.546	3.363	3.505	3.505			
c	5.451	5.609	5.451	5.549	5.549			
B_0	41.51	43.98	53.56	47.60		47.60	43.40	46.00
B_0'	3.53	1.22	2.88		2.8			

We presented two sets of calculation for exchange-correlation functionals. GGA calculation was obtained by using associated projectors as Custom, pseudo wave function as Polynom2, shape functions as Gaussian, $V_{PS}(r)$ (local) pseudopotential as UltraSoft and with parameters r_{paw} = 2.6 a.u. configuration to generate (smooth) pseudo partial-waves. LDA calculation was obtained by using associated projectors as Custom, pseudo wave function as Polynom2, shape functions as Sinc, $V_{PS}(r)$ (local) pseudopotential as TroullierMartins and with parameters r_{paw} = 2.4 a.u. configuration to generate (smooth) pseudo partial-waves. We used r_{paw} = 2.6 a.u. for GGA in the first calculation, while we used r_{paw} = 2.4 a.u. for LDA in the second calculation. We found lattice constant a

3.363 Å with error 4.1 % and c 5.451 Å with error 1.8 % with respect to experimental lattice constants 3.505 and 5.549 Å, and these were the same for GGA and LDA. GGA_{opt3} results were better than GGA and LDA. According to experimental values [150, 36], its results were 3.546 for lattice constant a with error 1.169 % and 5.609 Å for lattice constant c with error 1.1 %. Our bulk modulus calculations were computed as 41.51 GPa for GGA calculation, 43.98 GPa for GGA_{opt3} calculations, and 53.56 GPa for LDA calculations. Even though bulk modulus of GGA was agree well with theoretical value [41], it was not agree with known theoretical and experimental values. GGA_{opt3}, which was 1.4 % larger than theoretical value 43.40 GPa [41] and was smaller 4.4 % than theoretical value 46.00 GPa [148], these were resemble with theoretical value, but not agree with experimental value. Bulk modulus result of LDA was agree neither experimental nor theoretical values. Although pressure derivative of bulk modulus for LDA was closely resemble with experimental value [150], the others calculations were not similar with experimental value. LDA was computed as 2.88 with error 2.9 %.

Table 4.29: Total energy for nonmagnetic and ferromagnetic ground state (eV) of Lutetium

	Non magnetic	Ferro magnetic	ΔE (E_{NM}-E_{FM})
GGA	-15110.5119	-15110.5029	-0.0090
LDA	-15135.5688	-15135.5683	$-5.3e^{-4}$

Since the non-magnetic ground-state energy is lower than the energy of the ferromagnetic structure. The theoretical ground state is non-magnetically ordered in the experimental case, also for GGA. For LDA, the difference between the total energies of non-magnetic and ferromagnetic states is $-5.3e^{-4}$ (eV) which is less than the energy resolution of our calculations. Thus, it is not possible to make a distinction between those states theoretically.

CHAPTER 5

CONCLUSION

In this thesis, we have studied elemental and atomic properties of 4f series such as lattice constant, bulk modulus, and its pressure derivatives within PAW method framework within GGA (Perdew-Burke-Ernzerhof) and LDA (Perdew-Wang) exchange-correlation functionals. First of all, we have determined the best pseudopotential of GGA and LDA for each element, in this stage pseudopotential functions, projector choose, orthogonal functions, and shape functions are highly important for pseudopotential generation. After these functions have specified, we have measured the lattice constant of elements in order to compute bulk modulus and electronic density of state calculations. We determine the bulk modulus and its pressure derivatives with the aid of Vinet equation of state adapted to fit total energies. Lattice constants and bulk modulus calculations are agreement with experimental and theoretical results. Lattice constants results are agreement with experimental and theoretical results. La, Ce, Pr, Nd, Pm, Gd, Ho, Yb and Lu for GGA + U calculations are better than other elements according to experimental results. Sm, Eu, Tb, Dy, Er and Tm for LDA+ U results are agree with previous results. In this bulk modulus calculations we can see similarities except for Pm, Sm and Yb. We can say that GGA + U results are usually better than LDA +U results in lattice constants and bulk modulus results.

REFERENCES

[1] P. Hohenberg and W. Kohn, Phys. Rev. B **136**, 864 (1964).

[2] W. Kohn and L. J. Sham, Phys. Rev. 140, p. A1133 (1965).

[3] R. M. Martin, *Electronic Structure* Cambridge University Press (2004).

[4] N. W. Ashcroft and N. D. Mermin, *Solid State Physics* Harcourt College Publishers (1976).

[5] D. H. Hamann, M. Schluter and C. Chiang, Phys. Rev. Lett. **43**, 1494 (1979).

[6] P. E. Blöchl, Phys. Rev. B **50** , 17 953 (1994).

[7] V. Milman, B. Winkler, J. A. White, C. J. Pickard, M. C. Payne, E. V. Akhmatskaya and R. H. Nobes, International Journal of Quantum Chemistry, **77**, 895 - 910 (2000).

[8] D. Vanderbilt, Phys. Rev. Lett. **32**, 8415 (1985).

[9] D. Vanderbilt, Phys. Rev. Lett. **41**, 7892 (1990).

[10] G. Kresse and D. Joubert, Phys. Rev. B **59**, 1758 (1998).

[11] R. Car and M. Parrinello, Phys. Rev. Lett. **55**, 2471 (1985).

[12] P. E. Blöchl, Phys. Rev. Lett. **41**, 5414 (1990).

[13] N. A. W. Holzwarth, G. E. Matthews, R. B. Dunning, A. R. Tackett and Y. Zeng, Phys. Rev. B **55** , 2005 (1996).

[14] A. Zunger and M. L. Cohen, Phys. Rev. lett. **41**, 53 (1978).

[15] C. F. Melius and W. A. Goddard, Phys. Rev. A **10**, 1528 (1974).

[16] M. L. Cohen, Phys. Rev. Lett. **T1**, 5-10 (1982).

[17] C. Herring, Phys. Rev. **57**, 1169 (1940).

[18] J. C. Phillips and L. Kleinman, Phys. Rev. **116**, 287 (1959).

[19] M. L. Cohen and V. Heine, Phys. Rev. **122**, 1821 (1961).

[20] N. Troullier and J. L. Martins, Phys. Rev. B **43**, 1993 (1991).

[21] A. M. Rappe, K. M. Rabe, E. Kaxiras and J. D. Joannopoulos, Phys. Rev. B **41**, 1227 (1990).

[22] L. Kleinman and D. M. Bylander, Phys. Rev. Lett. **48**, 1425 (1982).

[23] X. Gonze and F. Finocchi, Physica Scripta. **T109**, 40-47 (2004).

[24] D. Cunnama, *The effect of the f-component of the pseudopotential on selected properties of 5d transition metal systems*, Pietermaritzburg August, (2008).

[25] C. M. Sturza, R. Boscence and V. Nacea, Farmacia **LVI** , 3, (2008).

[26] *http://metals.about.com/od/properties/a/Rare-Earth-Elements-Rees.htm.*

[27] H. Jiang, P. Rinke and M. Scheffler, Phys. Rev. B **sub**, APRIL 13 (2012).

[28] *http://chemistry.about.com/od/elementgroups/a/lanthanides.htm.*

[29] *http://www.tutorsonnet.com/chemistry homework help/inorganic chemistry/periodic table/f block/general characteristics of lanthanides assignment help tutoring.htm.*

[30] K. H. J. Buschow, *Handbook of Magnetik Materials*, Volume 13.

[31] J. C. G. Bünzli, Acc. Chem. Res. **39** , 53-61 (2006).

[32] *http://www.transtutors.com/chemistry-homework-help/d-and-f-block-elements/lanthanides.aspx.*

[33] B. Johansson and A. Rosengren, Phys. Rev. B **11**, 2836 (1975).

[34] K. A. Gschneidner, Jr., Rare Earth Alloys (D. Van Nostrand Company, Princeton, New Jersey, (1961).

[35] D. B. Mcwhan and A. L. Stevens, Phys. Rev. **139**, 3A, (1965).

[36] D. R. Lide, (Ed.) and W. M. Mickey Haynes(Ass. Ed.) CRC Handbook of Chemistry and Physics, 90^{th} Edition, (2010).

[37] K. Takemura and K. Syassen, J. Phys. F: Met. Phys. **15** 543-559 (1985).

[38] D. R. Stephens, J. Phys. Chem. Solids **25** 423 (1964).

[39] C. E. Montfort and C. A. Swenson, J. Phys. Chem. Solids **26** 623 (1965).

[40] D. B. McWhan, P. C. Sours and G. Jura, Phys. Rev. **143** 385 (1966).

[41] P. W. Bridgman (1964) Collected Experimental Papers (Cambridge. Mass.: Harvard University Press).

[42] G. Kotliar, *Strongly correlated electrons: a dynamical mean field perspective* , Center for Materials Theory and Physics Department Rutgers University, Piscataway NJ 0854, USA.

[43] E. Dagotto and Y. Tokura, *A brief introduction to strongly correlated electronic materials*, lecture note.

[44] V. Anisimov and Y. Izyumov, *Electronic Structure of Strongly Correlated Materials* , Springer Series in solid-state science.

[45] Z. Yin, *Microscopic Mechanisms of Magnetism and Superconductivity Studied from First Principle Calculations* , Phd Thesis, (2009).

[46] G. Kotliar and D. Vollhardt, *Strongly Correlated Materials: Insights From Dynamical Mean-Field Theory* , American Institute of Physics, (2004).

[47] Z. W. Lu, David, J. Singh and H. Krakauer, Phys. Rev. B **39**, 8 (1989).

[48] S. Li-Li, J. Guang-Fu, C. Xiang-Rong and G. Qing-Quan, Chin. Phys. Lett. **26**, 017101 (2009).

[49] J. K. Baria and A. R. Jani, Physica B **405**, 2065-2071 (2010).

[50] J. K. Baria and A. R. Jani, Pramana -J. Phys **60**, 1235-1246 (2003).

[51] B. Amadon, F. Jollet and M. Torrent, Phys. Rev. B **77**, 155104 (2008).

[52] A. B. Shick, A. I. Liechtenstein and W. E. Pickett, Phys .Rev. B **60**, 15 (1999).

[53] A. M. Vora, Central European Journal of Physics.

[54] S. Bağcı, H. M. Tütüncü, S. Duman and G. P. Srivastava, Phys. Rev. B **82**, 144507 (2010).

[55] M. Hülsen, A. Weigand and M. Dolg, Theor. Chem. Account. **122**:23-29 (2009).

[56] L. Huang and C. A. Chen, J. Phys.: Condens. Matter **19**, 476206 (12pp) (2007).

[57] C. Hartwigsen, S. Goedecker and J. Hutter, Phys. Rev. B **58**, 3641 (1998).

[58] C. Loschen, J. Carrasco, K. M. Neyman and F. Illas, Phys. Rev. B **75**, 035115 (2007).

[59] J. Long, Physica B **407** 4831-4836 (2012).

[60] Y. Makino, Journal of Alloys and Compounds, 408-412, 484-489 (2006).

[61] P. B. Thakor, P. N. Gajjar and A. R. Jani, Commun. Theor. Phys. **46**, 337-342 (2006).

[62] Y. Wang and M. Dolg, Theoretical Chem. Acc. **100**, 124-133 (1998).

[63] Y. Makino, Journal of Alloys and Compounds **242**, 122-128 (1996).

[64] Z. Jian-Zhou, Z. Jia-Ning, D. Xiao-Yu, B. Yan, C. Ling-Cang, F. Zhong and D. Xi, Chin. Phys. B Vol. **21**, 057106 (2012).

[65] G. Y. Gao, Y. L. Niu, T. Cui, L. J. Zhang, Y. Li, Y. Xie, Z. He, Y. M. Ma and G. T. Zou, J. Phys.: Condens. Matter **19**, 425234 (9pp) (2007).

[66] N. Singh and S. P. Singh, Phys. Rev. B **42**, 3 (1990).

[67] H. M. Tütüncü and G. P. Srivastava, Journal of applied physics **104**, 063916 (2008).

[68] N. V. Skorodumova, R. Ahuja, S. I. Simak, I. A. Abrikosov, B. Johansson and B. I. Lundqvist, Phys. Rev. B **64**, 115108 (2001).

[69] F. D. Stacey, B. J. Brennan, R. D. Irvine, and G. Surveys, **4** 189 (1981).

[70] O. L. Anderson, Oxford University Press, New York (1995).

[71] S. Gaurav, B. S. Sharma, S. B. Sharma and S. C. Upadhyaya, Physica B **322** , 328-339 (2002).

[72] G. Parsafar and E. A. Mason, Phys. Rev. B **49** 5 3049 (1994).

[73] P. Vinet, J. R. Smith, J. Ferrante and J. H. Rose, Phys. Rev. B **35** 1945 (1987).

[74] P. Kuchhal and N. Dass, Pramana journal of physics 61 (2003).

[75] P. Vinett, J. Ferrante, J. R. Smith and J. H. Rose, J. Phys. C: Solid State Phys. 19 (1986).

[76] F. D. Murnaghan, Wiley, NY (1951).

[77] M. Braithwaite, C. E. Sims and N. L. Allan, CP620, Shock Compression of Condensed Matter (2001).

[78] S. Digpratap, K. Sushil and B. P. Singh Department, Indian Journal of Pure and Applied Physics **45** 721-725 (2007).

[79] S. Ozgen, L.Songur and I. Kara, Turk J. Phys, **36** (2012).

[80] M. S. Kumar and B. S. Sharma, Indian Journal of Pure and Applied Physics 48, (2010).

[81] S. S. Kushwah and J. Shanker, Physica B 253 (1998).

[82] R. D.Cowan and W. Fickett, J Chem Phys **24**, 932 (1956).

[83] G. Parsafar and E. A. Mason, Phys Rev B **49** 3049-3060 (1994).

[84] J. Hama and K. Suito, J Phys, **8** 67 (1996).

[85] P. B. Roy and S. B. Roy, Physica B, 350 (1945).

[86] J. Shanker, Physica B, 271 , 158 (1999).

[87] R. Rydberg, J Phys, 73 376 (1932).

[88] P. B. Roy and S. B. Roy, Phys Status Solid, 226 125 (2001).

[89] S. S. Kushwah and Y. S. Tomar, Indian Journal of Pure and Applied Physics 49, (2011).

[90] *A Lanthanide Lanthology*, Molycorp, Inc. Mountain Pass, CA, U.S.A.

[91] L. W. Nixon, D. A. Papaconstantopoulos and M. J. Mehl, Phys. Rev. B **78**, 214510 (2008).

[92] The ABINIT code is a common project of the Universite Catholique de Louvain, Corning Incorporated, and other contributors (www.abinit.org); see X. Gonze, J. M. Beuken, R. Caracas, F. Detraux, M. Fuchs, G.M. Rignanese, L. Sindic, Verstraete M, Zerah G, Jollet F, Torrent M, Roy A, M. Mikami, Ph. Ghosez, J. Y. Raty and D. C. Allan, Comput. Mater. Sci. **25**, 478 (2002).

[93] A. Delin, L. Fast, B. Johansson, O. Eriksson and J. M. Wills, Phys. Rev. B **58**, 4345 (1998).

[94] Z. W. Lu, D. J. Singh and H. Krakauer, Phys. Rev. B **39**, 4921 (1998).

[95] A. H. Daane, in The Rare Earths, edited by F. H. Spedding and A. H. Daane (Wiley, New York, 1961), p. 182.

[96] K. Syassen and W. B. Holzapfel, Solid State Commun. **16**, 533 (1975).

[97] C. Kittel, Introduction to Solid State Physics, 7th ed. (Wiley, New York, 1996), p. 59.

[98] B. T. Kilbourn, Cerium a Guide to its Role in Chemical Technology, booklet publ. Molycorp, (1993) (available on request).

[99] R. F. Gempel, D. R. Gustafson and J. D. Willenberg, Phys. Rev. B **5**, 2082 (1972).

[100] E. Franceschi and G. L. Olcese, Phys. Rev. Lett. **22**,1299 (1969).

[101] B. L. Davis and L. H. Adams, J. Phys. Chem. Solids **25**, 379 (1964).

[102] D. B. McWhan, Phys. Rev. B **1**, 2826 (1970).

[103] A. W. Lawson and T. Y. Tang, Phys. Rev. B **76**, 301 (1949).

[104] N. Richard and S. Bernard, Journal of Alloys and Compounds **628 - 631**, 323 - 324 (2001).

[105] C. Stassis, T. Gould, O. D. McMasters, K. A. J. Gschneidner and R. M. Nicklow, Phys. Rev. B **19** 5746 (1979).

[106] J. S. Olsen, L. Gerward, U. Benedict and J. P. *Itié*, Physica B+C **133B** 129 (1985).

[107] A. Svane, Phys. Rev. B **53**, 4275 (1996).

[108] A. B. Shick, W. E. Pickett and A. I. Liechtenstein, J. Electron Spectrosc. Relat. Phenom. **114 - 116** 753 (2001).

[109] L. Huang and C. A. Chen, J. Phys.: Condens. Matter **19** 476206 (12pp) (2007).

[110] K. A. Gschneidner, Solid State Phys. **16** 275 (1964).

[111] O. Eriksson, M. S. S. Brooks and B. Johansson, Phys. Rev. B **41** 10 (1990).

[112] I. K. Jeong, T. W. Darling, M. J. Graf, T. Proffen, R. H. Heffner, Y. Lee, T. Vogt and J. D. Jorgensen, Phys. Rev. Lett. **92**, 105702 (2004).

[113] P. Soderlind, O. Eriksson, B. Johansson and J. M. Wills, Phys. Rev. B **50**, 7291 (1994).

[114] P. Ravindran, L. Nordström, R. Ahuja, J. M. Wills, B. Johansson and O. Eriksson, Phys. Rev. B **57**, 2091 (1998).

[115] B. Johansson, I. A. Abrikosov, M. Aldén, A. V. Ruban and H. L. Skriver, Phys. Rev. Lett. **74**, 2335, (1995).

[116] G. N. Chesnut and Y. K. Vohra, Phys. Rev. B **61** R3768 (2000).

[117] U. Lundin, I. Sandalov, O. Eriksson and B. Johansson, Solid State Communications **115** 7-12 (2000).

[118] Y. I. Spichkin, J. Bohr and A. M. Tishin, Phys. Rev. B **54** 9 (1996).

[119] J. C. G. Hqoumann and R. M. Nicklow, Phys. Rev. B **1** 3943 (1970).

[120] O. Steinsvoll, G. Shirane, R. Nathans, M. Blume, H. A. Alpkrin and S. J. Pickart, Phys. Rev. **161** 499 (1967).

[121] W. M. Temmerman and P. A. Sterne, J. Phys. Condens. Matter **2**, 5529 (1990).

[122] D. C. Douglass, A. J. Cox, J. P. Bucher and L. A. Bloomfield, Phys. Rev. B **47** 19 (1993).

[123] Z. Klemm and H. Bommer, Z. anorg. u. allgem. Chem. **231** 138 (1937).

[124] Urbain, Weiss and F. Trombe, Compt. rend. **200**, 2132 (1935).

[125] F. Trombe, Ann. phys. **7**, 383 (1937).

[126] J. R. Banister, S. Legvold and F. H. Spedding, Phys. Rev. **94**, 5 (1954).

[127] S. B. Palmer, E. W. Lee and M. N. Islam, Proc. R. Soc. London, Ser. A **338**, 341 (1974).

[128] L. Roeland, G. Cock, F. Muller, A. Moleman, K. McEwen, R. Jordan and D. Jones, J. Phys. F **5**, L233 (1975).

[129] D. J. Singh, Phys. Rev. B **44**, 7451 (1991).

[130] M. Rosen, Phys. Rev. **174**, 504 (1968).

[131] M. Heinemann and W. M. Temmerman, Phys. Rev. B **49**, 4348 (1994).

[132] M. Heinemann and W. M. Temmerman, Phys. Rev. B **52**, 4420 (1995).

[133] A. B. Shick, A. I. Liechtenstein and W. E. Pickett, Phys. Rev. B **60**, 10 763 (1999).

[134] J. F. Elliqtt, S. Legvold and F. H. Spedding, Phys. Rev. **91**, 28 (1953).

[135] F. Trombe, J. phys. et radium **12**, 222 (1951).

[136] J. F. Elliqtt, S. Legvold and F. H. Spedding, Phys. Rev. **94**, 1143 (1954).

[137] B. A. H. Daane, R. E. Rundle, H. G. Smith and F. H. Spedding, Acta Cryst. **7** 32 (1954).

[138] G. Helgesen, J. P. Hill, T. R. Thurston, Doon Gibbs, J. Kwo and M. Hong, Phys. Rev. B **50** 5 (1994).

[139] R. M. Nicklow, N. Wakabayashi and P. R. Vijayaraghavan, Phys. Rev. B **3** 1229 (1971).

[140] W. C. Kohler, J. W. Cable, M. K. Wilkinson and E. O. Wollan, Phys. Rev. **151** 414 (1966).

[141] D. Gibbs, D. E. Moncton, K. L. D'Amico, J. Bohr and B. H. Grier, Phys. Rev. Lett. **55** 234 (1985).

[142] P. B. Fynbo, J. Phys. F: Metal Phys. **7** 10 (1977).

[143] T. O. Brun and G. H. Lander, Phys. Rev. Lett. **23** 1295 (1969).

[144] W. C. Koehler, J. W. Cable, E. O. Wollan and M. K. Wilkinson, Phys. Rev. **126** 1672 (1962).

[145] http://www.webelements.com/

[146] D. Andrae and B. Paulus, *The Crystal Structure of the Close-Packed Polymorphs of Ytterbium: A Quantum Chemical Study* Proceedings- 34^{TH} Annual Condensed Matter and Materials Meeting - Waiheke Island, Auckland, 2010.

[147] H. Cox, R. L. Johnston and A. Ward, J. Phys.: Condens. Matter **10** (1998) 9419-9429. Printed in the UK.

[148] L. G. Liu, J. Phys. Chem. Solids **36** 31 (1975).

[149] R. Rao and A. Ramanand, Phys. Status Solidi b **122** 11 (1984).

[150] N. Gonzalez Szwacki and T. Szwacka, Basic Elements of Crystallography, July (2009).

CHAPTER 6
APPENDIX

In this section, we have given fit result of EOS to show energy difference with respect to unit cell volume of lanthanides as well as all electron wavefunctions, pseudowave functions, projector wave functions, these wavefunctions are obtained to solution of schrödinger equation, and logarithmic derivatives of these wave functions of all elements in this study. It should be noted that the fitted equilibrium lattice parameters are highly dependent on the range of calculated volume-energy data sets. We can see this change in the below Figures, which are energy difference with respect to unit cell volume figures.

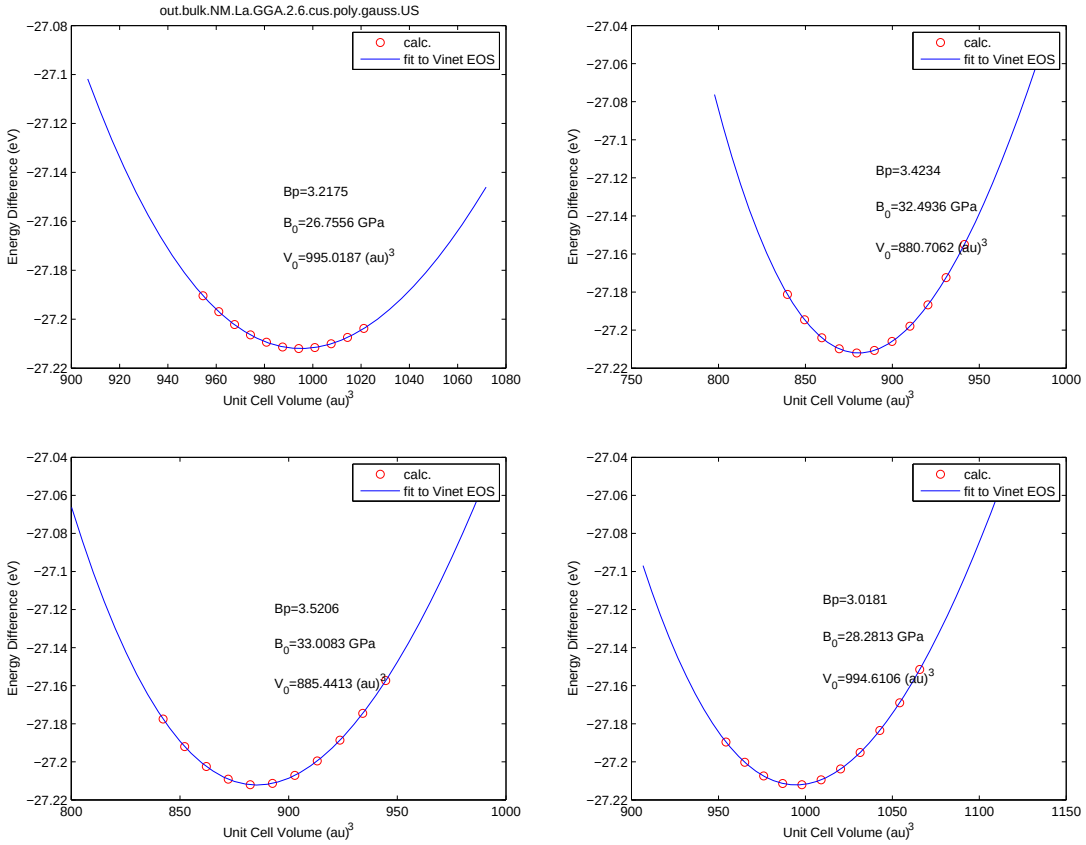

Figure 6.1: Energy difference with respect to unit cell volume of Lanthanum

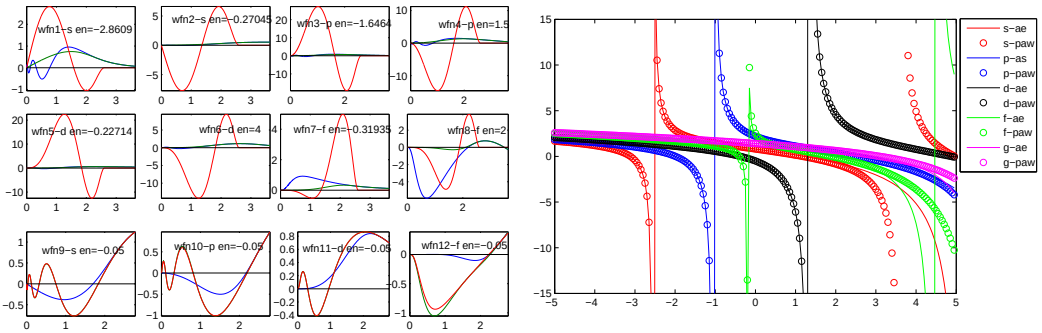

Figure 6.2: Wavefunctions and logarithmic derivatives of Lanthanum

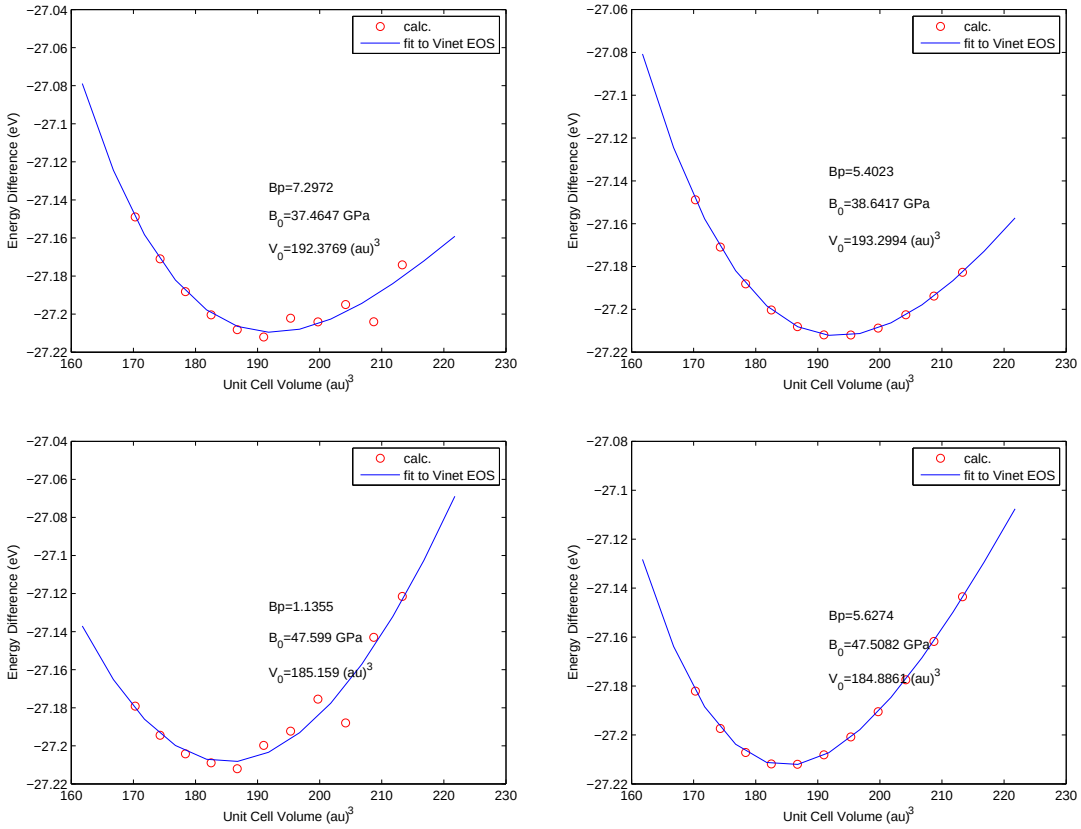

Figure 6.3: Energy difference with respect to unit cell volume of Cerium

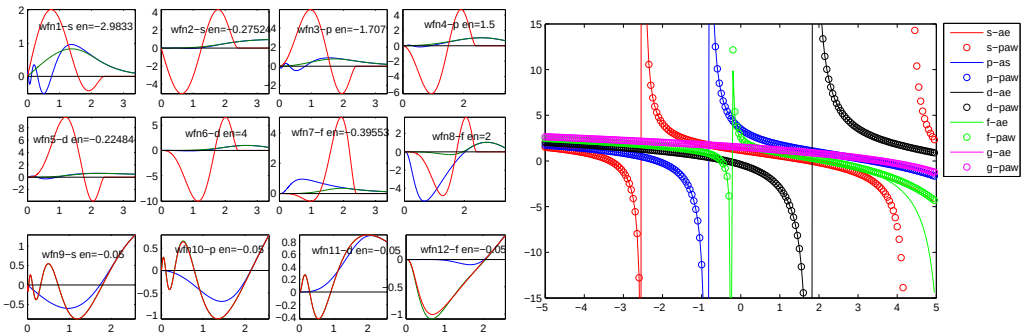

Figure 6.4: Wavefunctions and logarithmic derivatives of Cerium

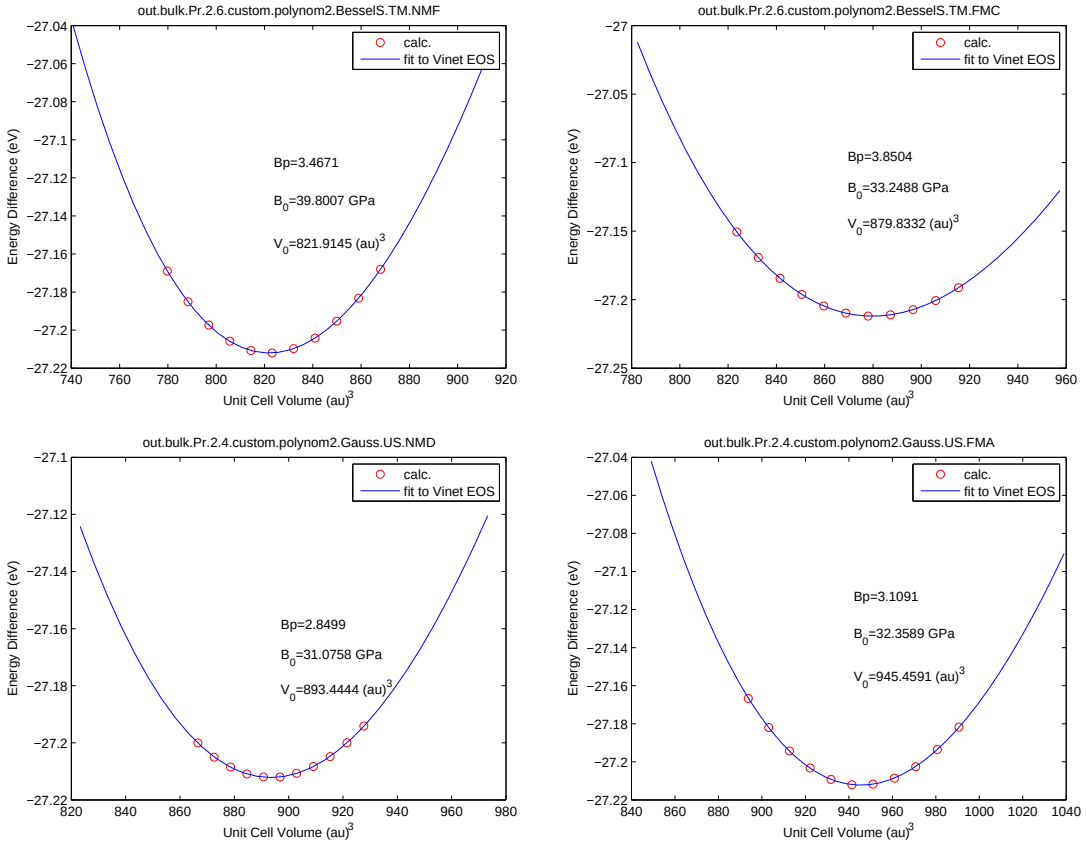

Figure 6.5: Energy difference with respect to unit cell volume of Praseodymium

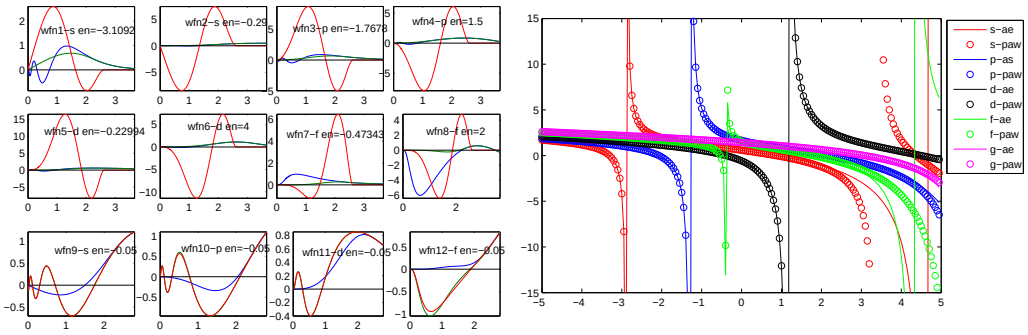

Figure 6.6: Wavefunctions and logarithmic derivatives of Praseodymium

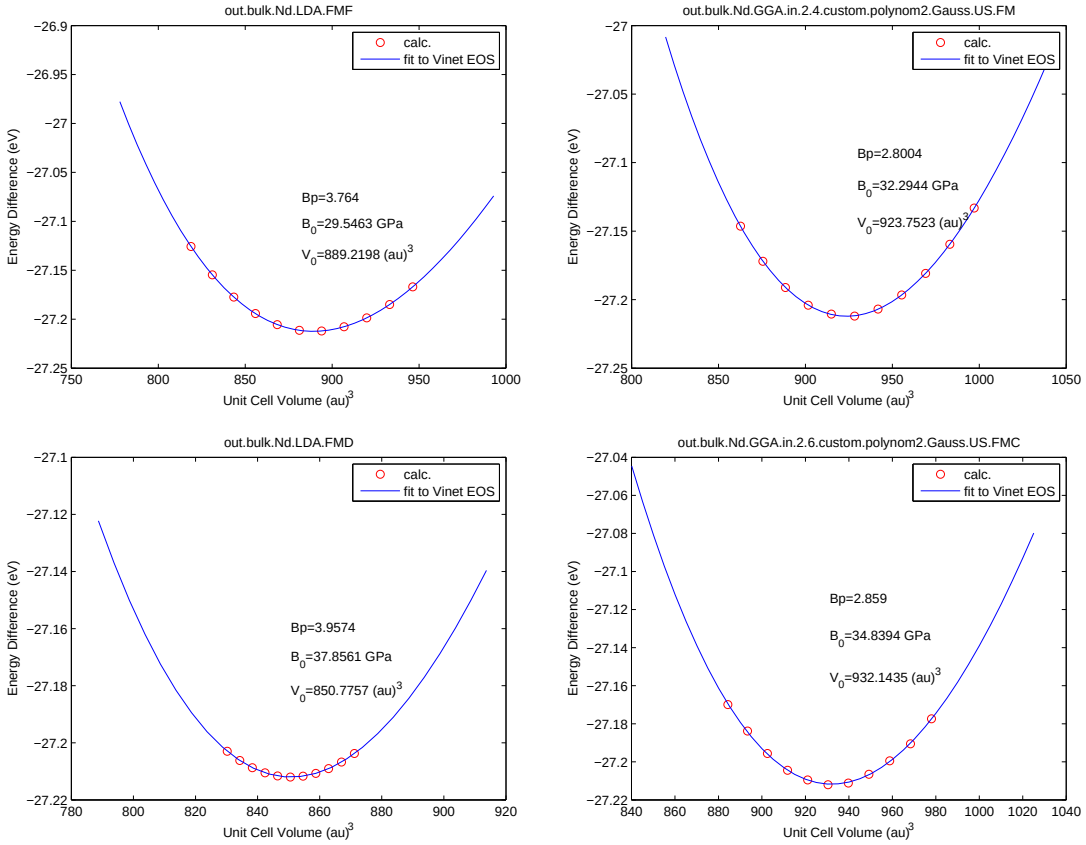

Figure 6.7: Energy difference with respect to unit cell volume of Neodymium

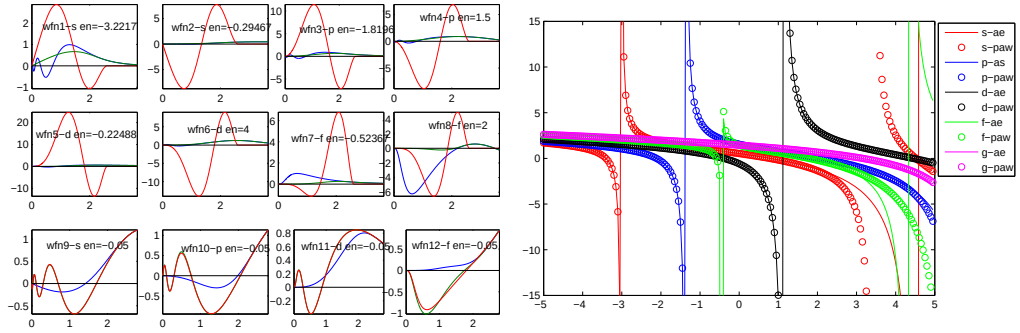

Figure 6.8: Wavefunctions and logarithmic derivatives of Neodymium

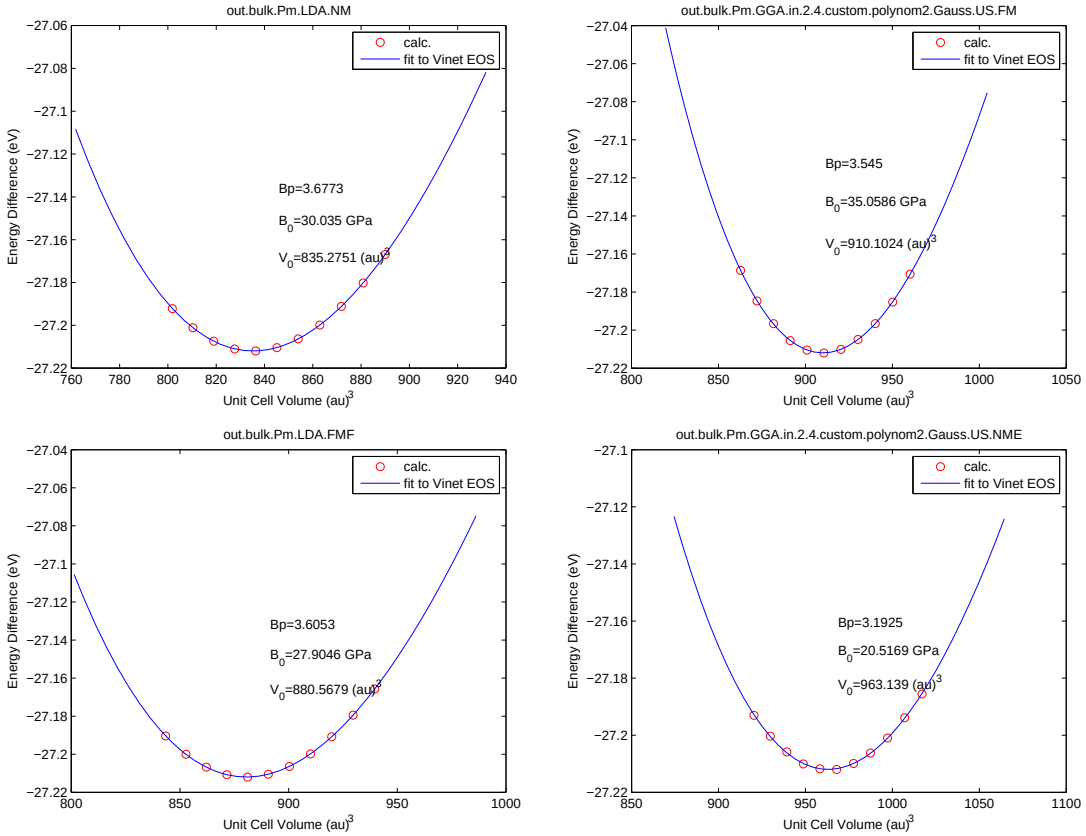

Figure 6.9: Energy difference with respect to unit cell volume of Promethium

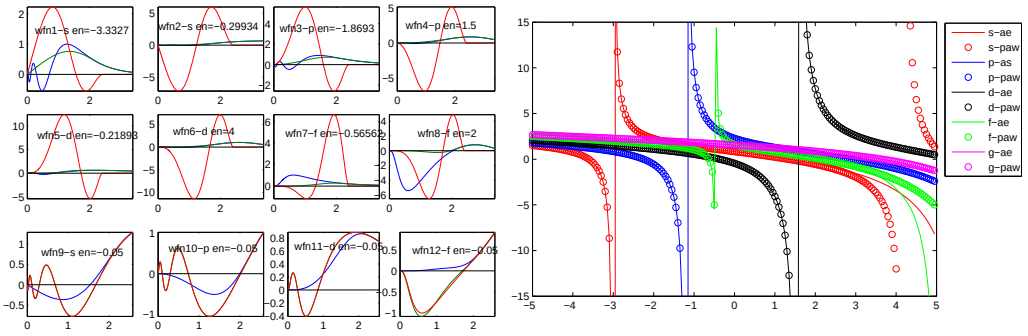

Figure 6.10: Wavefunctions and logarithmic derivatives of Promethium

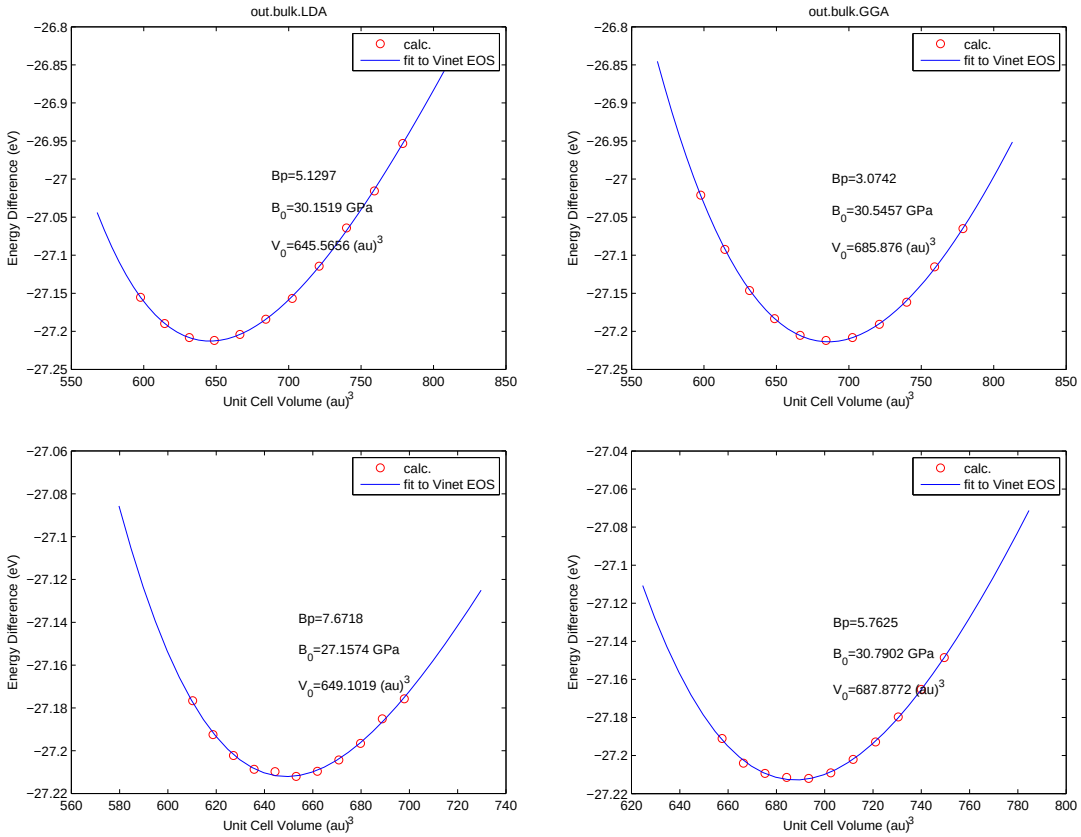

Figure 6.11: Energy difference with respect to unit cell volume of Samarium

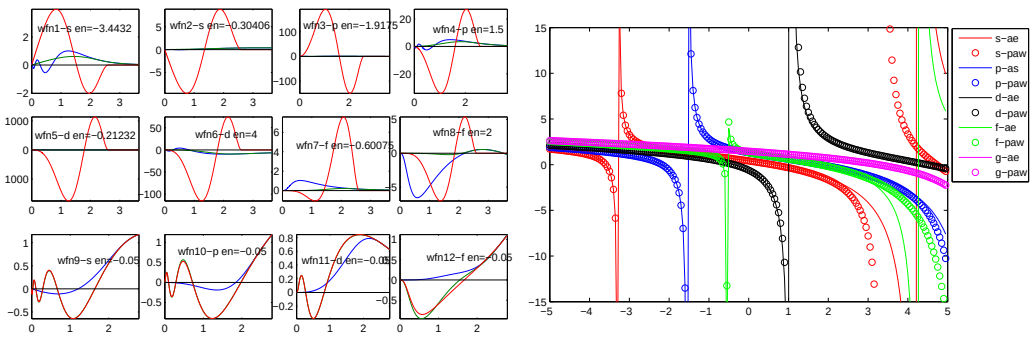

Figure 6.12: Wavefunctions and logarithmic derivatives of Samarium

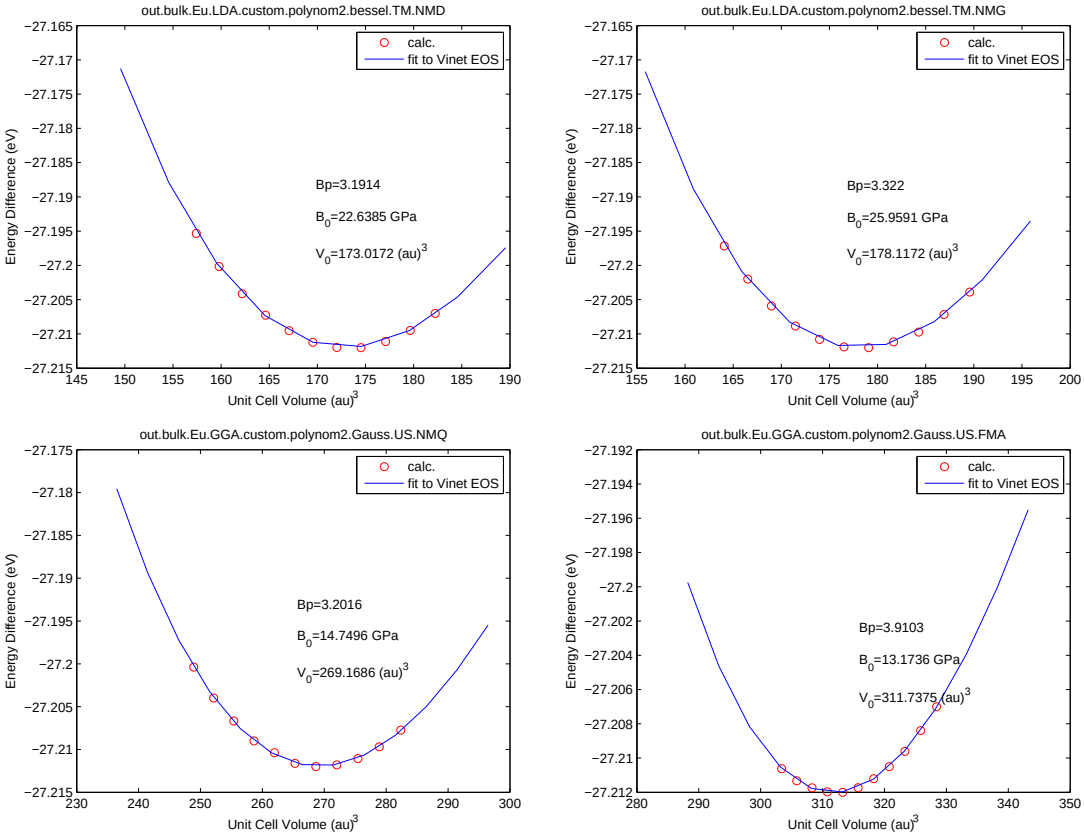

Figure 6.13: Energy difference with respect to unit cell volume of Europium

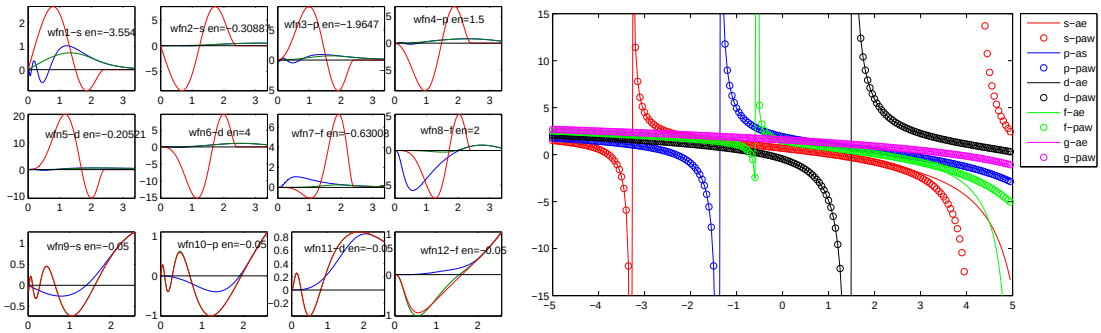

Figure 6.14: Wavefunctions and logarithmic derivatives of Europium

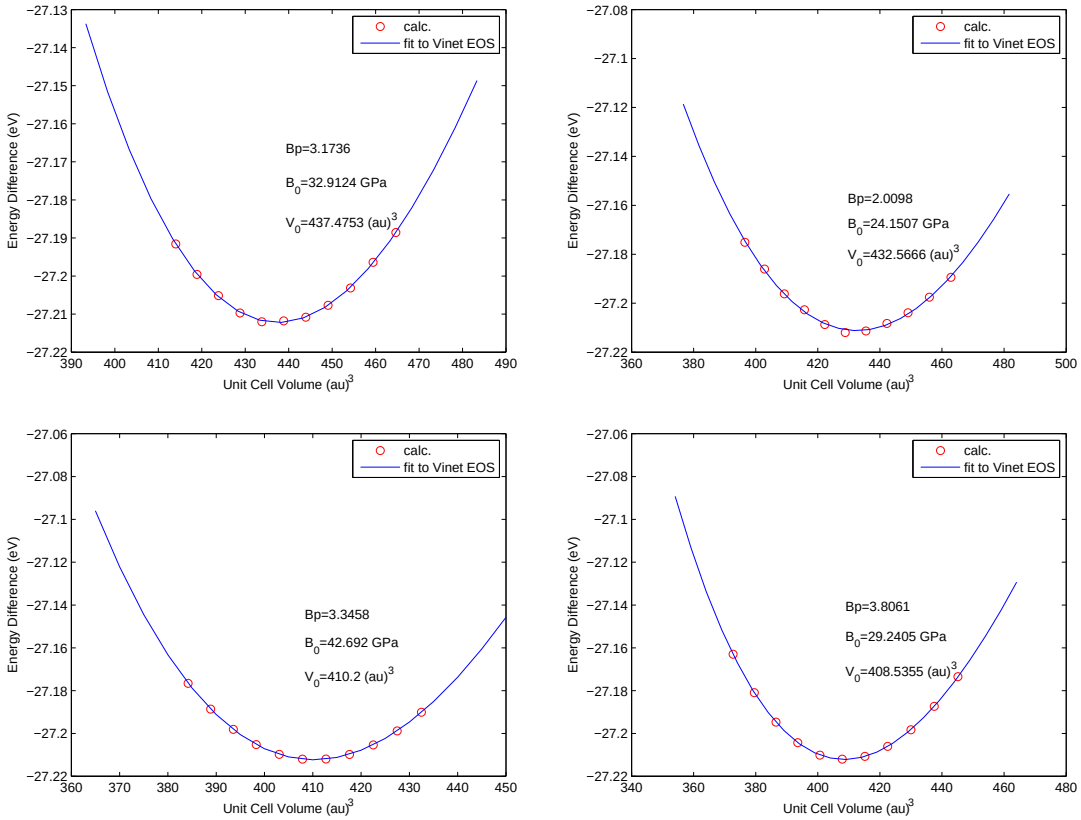

Figure 6.15: Energy difference with respect to unit cell volume of Gadolinium

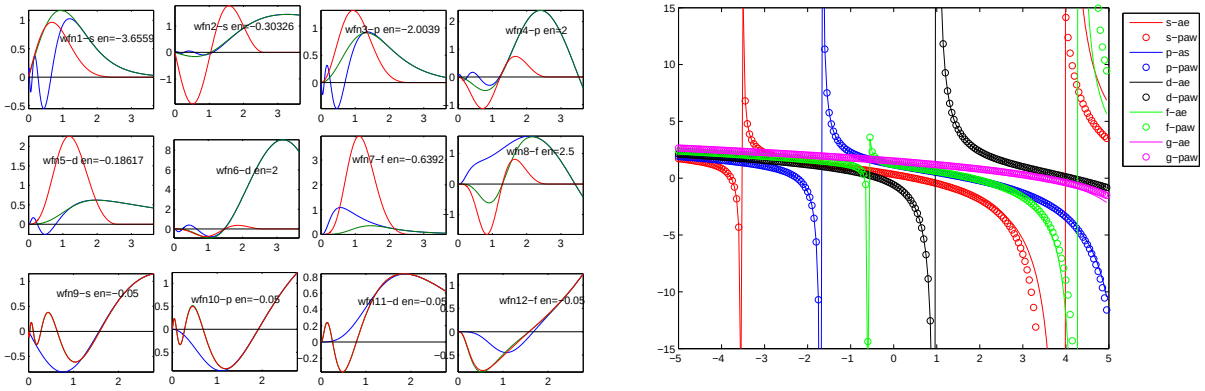

Figure 6.16: Wavefunctions and logarithmic derivatives of Gadolinium

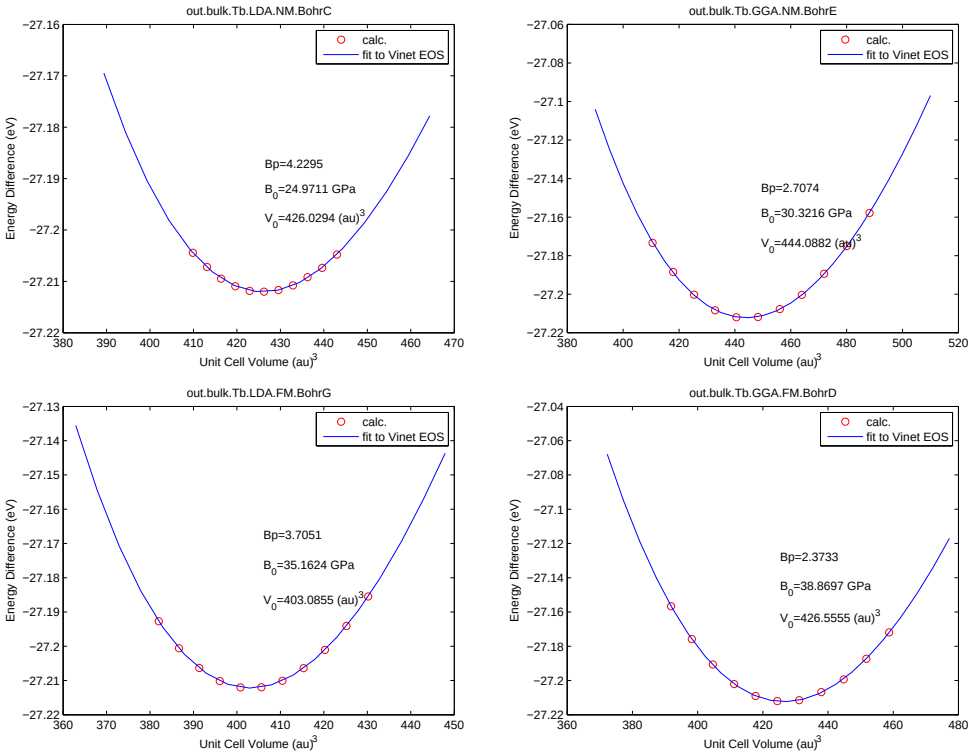

Figure 6.17: Energy difference with respect to unit cell volume of Terbium

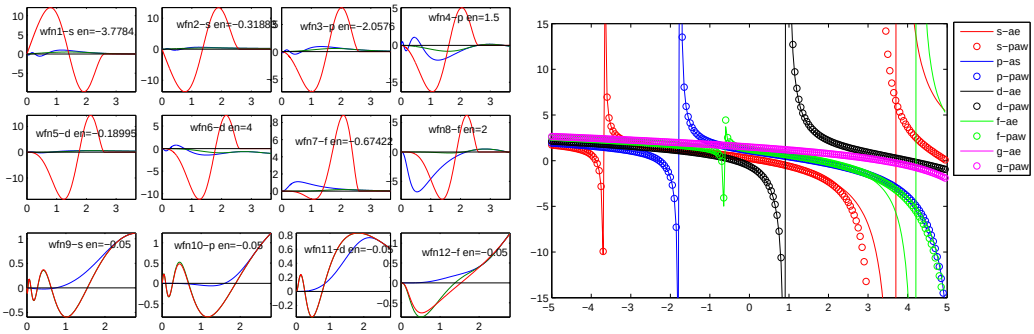

Figure 6.18: Wavefunctions and logarithmic derivatives of Terbium

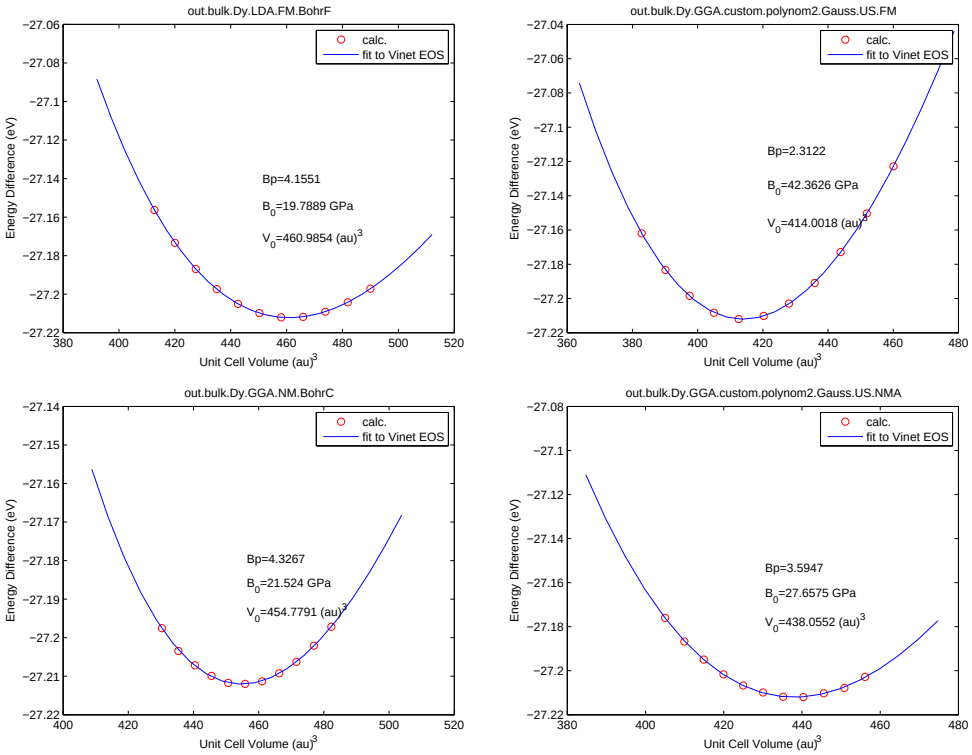

Figure 6.19: Energy difference with respect to unit cell volume of Dysprosium

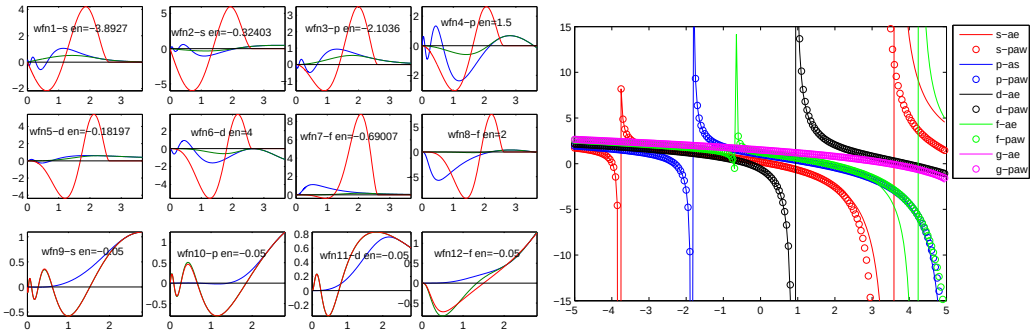

Figure 6.20: Wavefunctions and logarithmic derivatives of Dysprosium

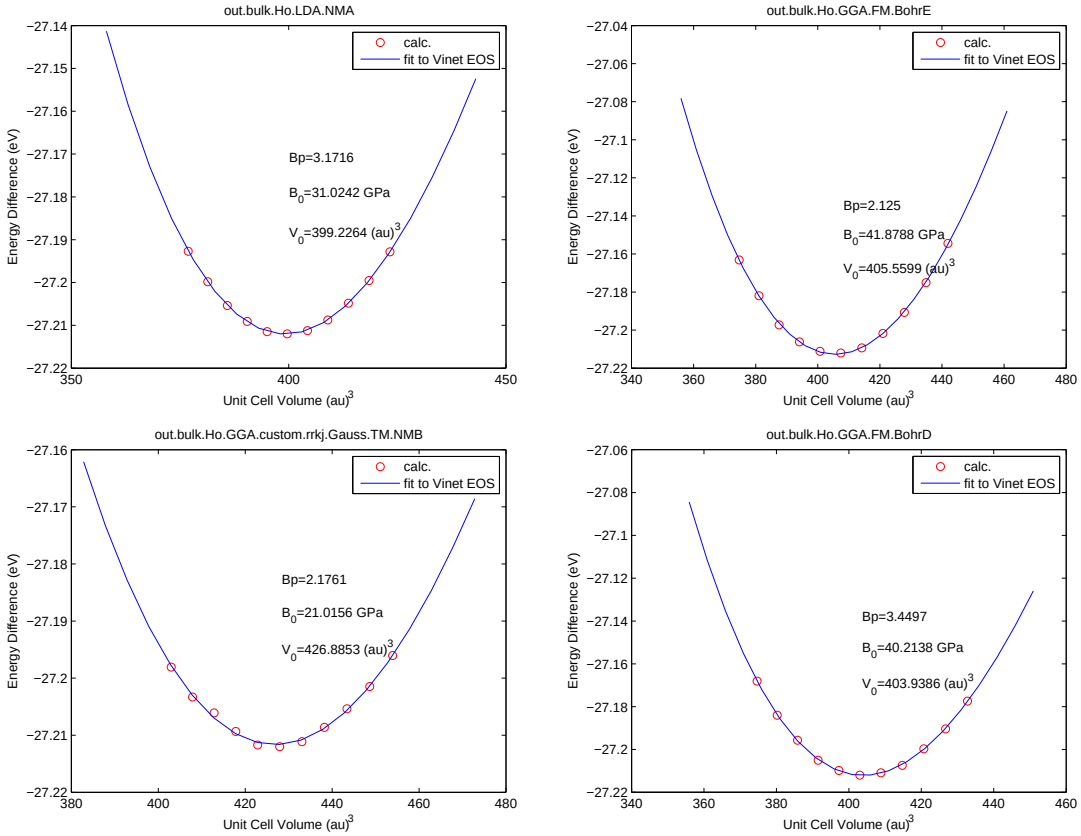

Figure 6.21: Energy difference with respect to unit cell volume of Holmium

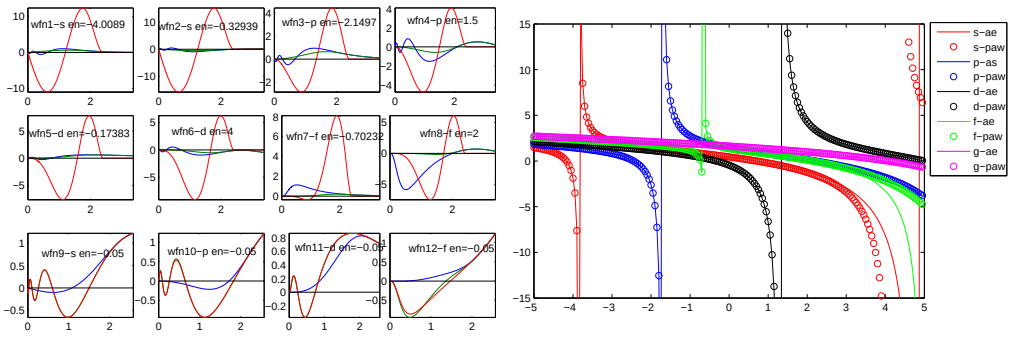

Figure 6.22: Wavefunctions and logarithmic derivatives of Holmium

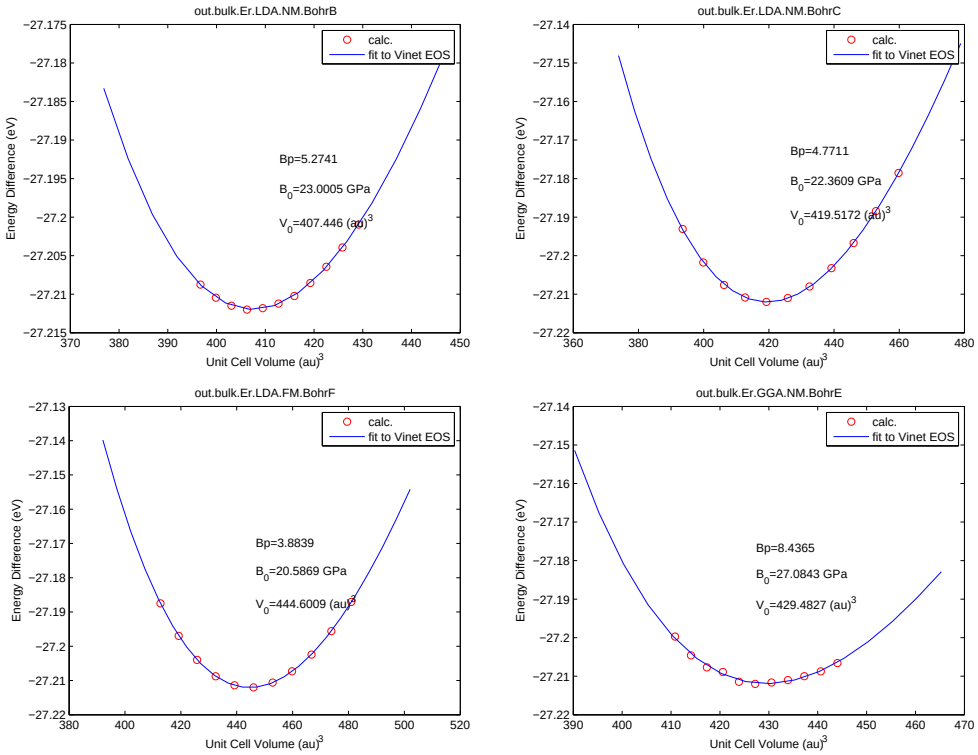

Figure 6.23: Energy difference with respect to unit cell volume of Erbium

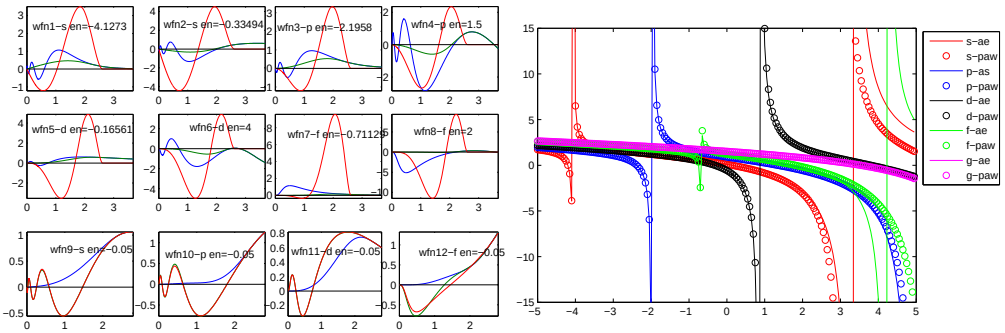

Figure 6.24: Wavefunctions and logarithmic derivatives of Erbium

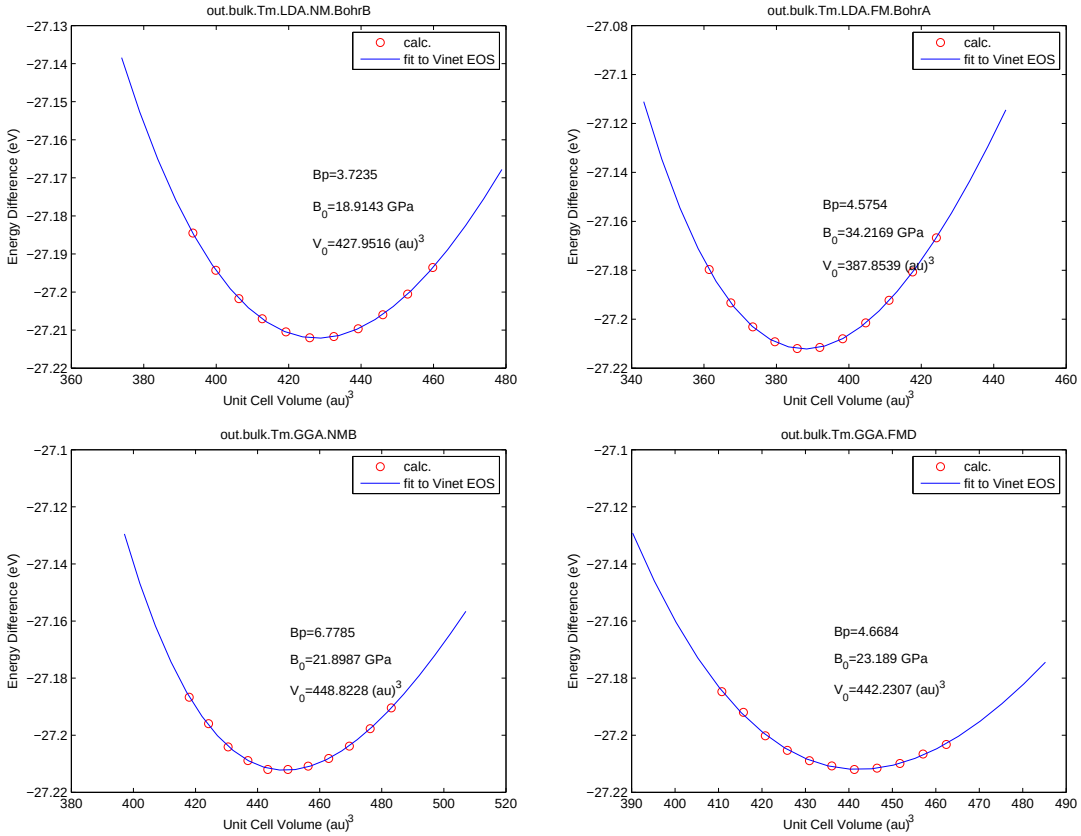

Figure 6.25: Energy difference with respect to unit cell volume of Thulium

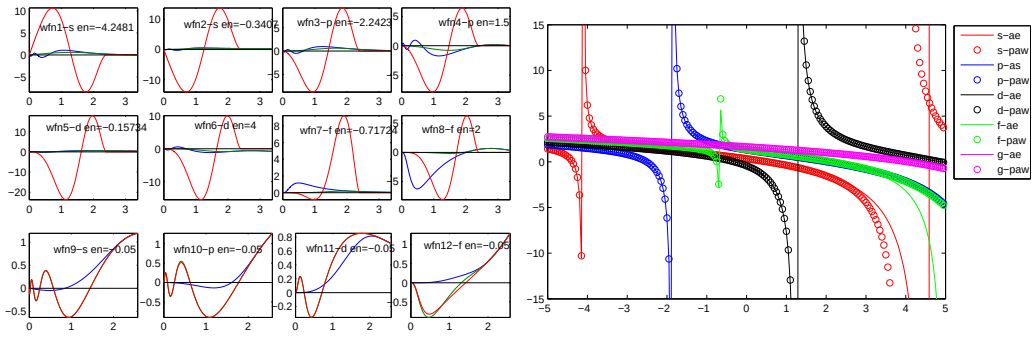

Figure 6.26: Wavefunctions and logarithmic derivatives of Thulium

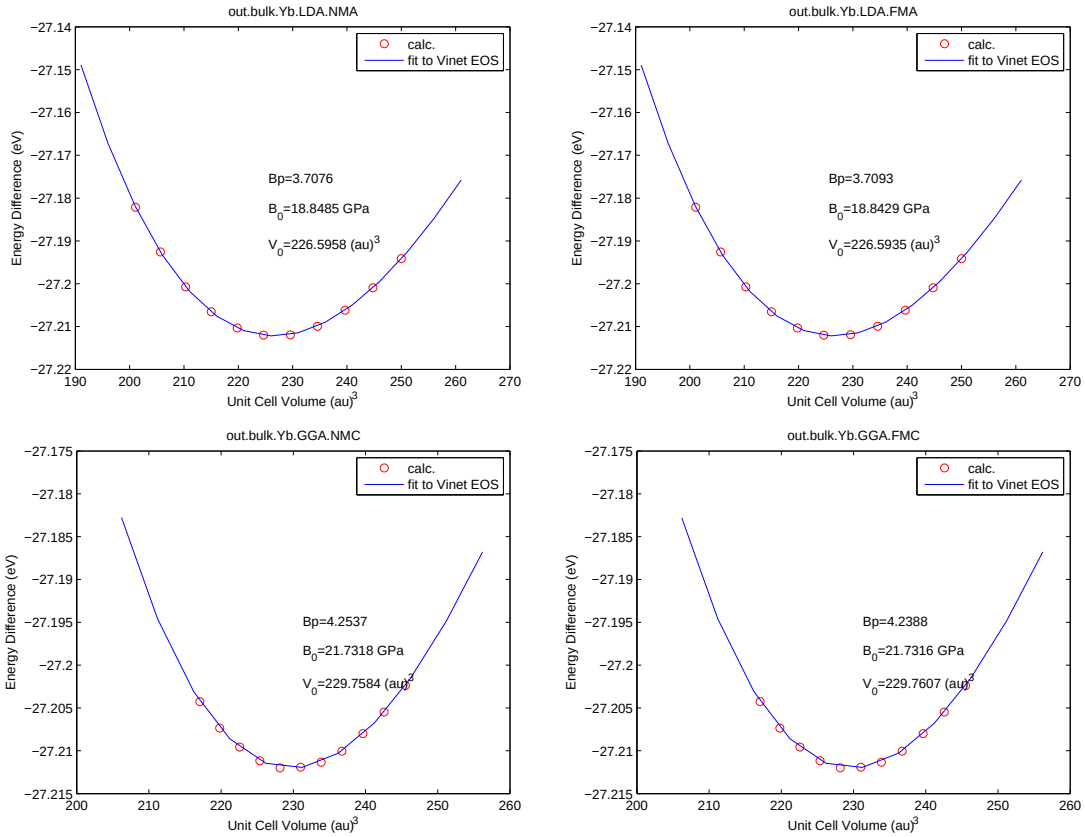

Figure 6.27: Energy difference with respect to unit cell volume of Ytterbium

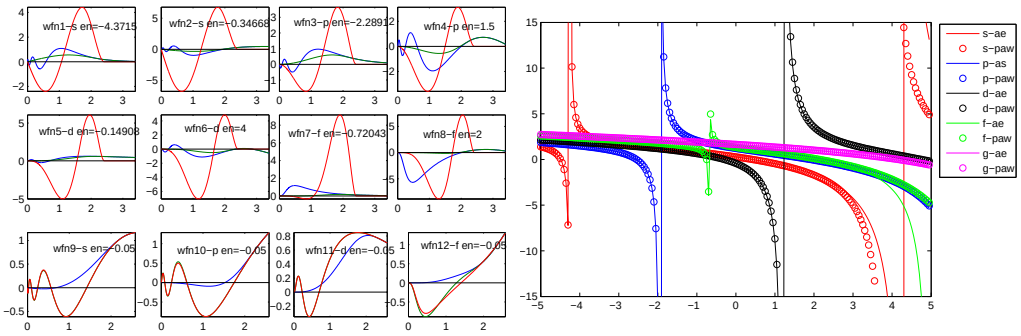

Figure 6.28: Wavefunctions and logarithmic derivatives of Ytterbium

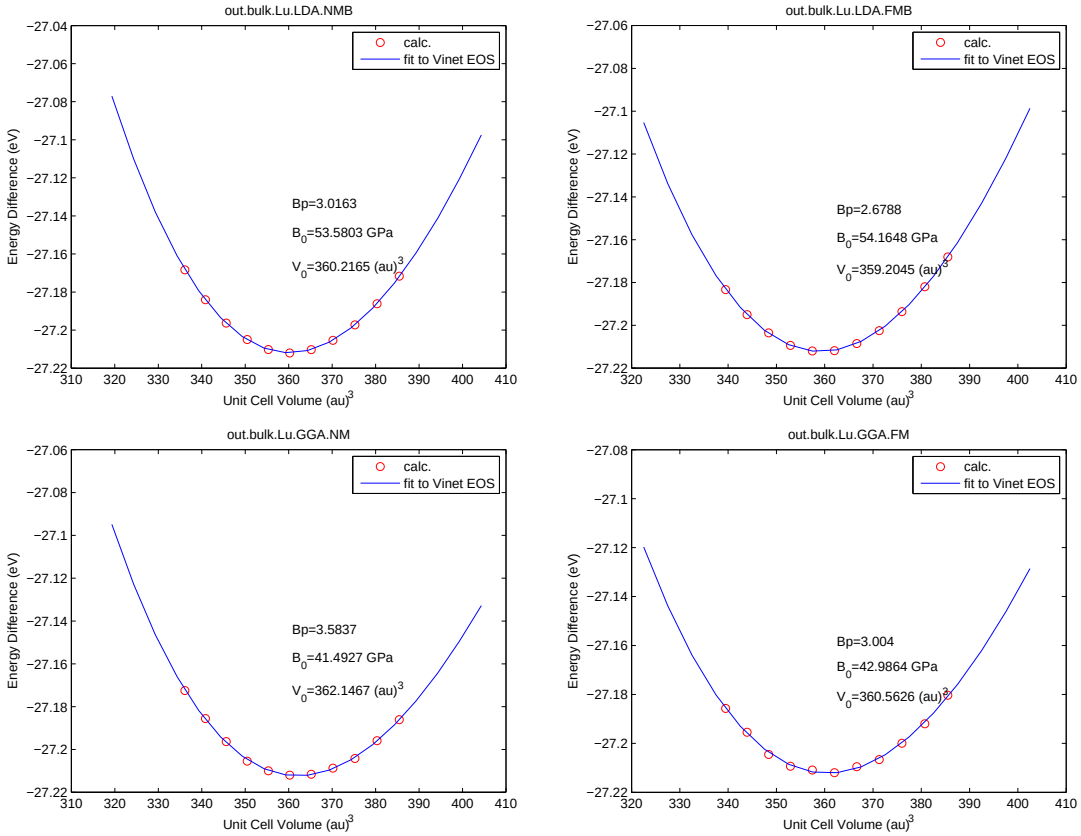

Figure 6.29: Energy difference with respect to unit cell volume of Lutetium

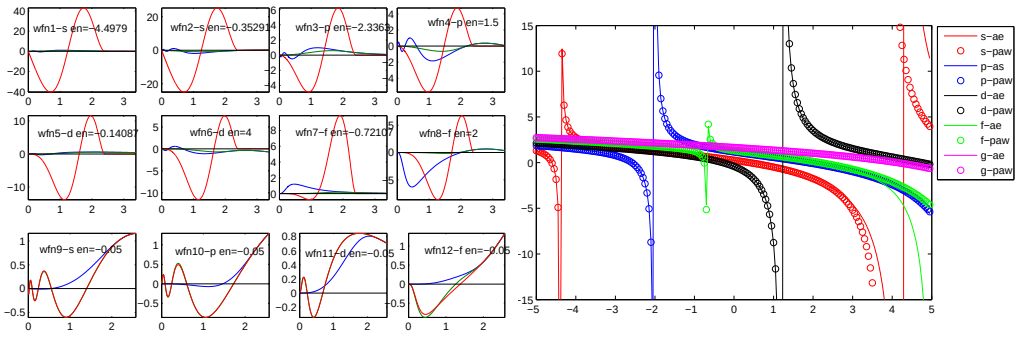

Figure 6.30: Wavefunctions and logarithmic derivatives of Lutetium

CURRICULUM VITAE

Güven AKÇAY

Address:

District: Çıkınlar,
Street: Büklüm, Number: 15,
City Center/Bolu, Turkey
Phone: 0538 835 20 41
Email: guvenakcayibu@gmail.com

Personal Details:

Gender: Male
Date of birth: 05th of October
Place of birth: Izmit, Turkey

Education:

2006-2011 Bachelor's Degree in Mathematics at Abant Izzet Baysal University

2009-2011 Bachelor's Degree in Second Major in Pyhsics at Abant Izzet Baysal University

2011-2012 Pedagogy Licence in Maths Teaching Education at Abant Izzet Baysal University

2011-2013 MSc in Pyhsics at Abant Izzet Baysal University
Thesis: 4f Series PAW Pseudopotentials

Publication:

Ertürk E., Gürel T., Lukoyanov A. V., Akçay G., Eryiğit R., Anisimov V. I. "Ab initio study on the rareearth ironpnictides RFeAsO (R = Pr, Nd, Sm, Gd) in the low temperature Cmma phase" J. Phys.: Condens. Matter 26, 045501 (2014).

Project:

"Influence of correlation effect on the electronic structure of superducting pnictidematerials" Tubitak, Grant No.111T796 (Researcher).